A High Resolution M Band Study of W3 IRS5

Kenneth Noel Belcourt

A thesis presented to the department of Astronomy, St. Mary's University, in partial fulfillment of the Master of Science degree.

© 1989 Kenneth N. Belcourt

National Library of Canada
Bibliothèque nationale du Canada

Canadian Theses Service
Service des thèses canadiennes

Ottawa, Canada
K1A 0N4

The author has granted an irrevocable non-exclusive licence allowing the National Library of Canada to reproduce, loan, distribute or sell copies of his/her thesis by any means and in any form or format, making this thesis available to interested persons.

The author retains ownership of the copyright in his/her thesis. Neither the thesis nor substantial extracts from it may be printed or otherwise reproduced without his/her permission.

L'auteur a accordé une licence irrévocable et non exclusive permettant à la Bibliothèque nationale du Canada de reproduire, prêter, distribuer ou vendre des copies de sa thèse de quelque manière et sous quelque forme que ce soit pour mettre des exemplaires de cette thèse à la disposition des personnes intéressées.

L'auteur conserve la propriété du droit d'auteur qui protège sa thèse. Ni la thèse ni des extraits substantiels de celle-ci ne doivent être imprimés ou autrement reproduits sans son autorisation.

ISBN 0-315-50914-7

Canada

Acknowledgements

A number of people have influenced my work in the 3 plus years I have been in Halifax. To name them all would be nigh on impossible so I won't attempt it, however, a few individuals deserve mention.

I would like to thank Dr. George Mitchell for suggesting this fascinating thesis project; your enthusiasm is contagious. I would also like to thank Dr. David Turner and Dr. Gary Welch for expanding the mind of yet another graduate student. Dr. (to be) Randall Brooks has been most helpful during my stay here. I would also like to thank Dr. Cameron Reed for many interesting discussions and for creating the title page to my thesis.

I also want to thank the many kind people who have made my stay here in the Maritimes really grand.

A special thanks to my fiancee, Carmenne Chiasson, for all her love and encouragment. I wonder how I ever got by before I met you.

Most importantly, I wish to thank my family for all their support and encouragement, and for being there when I needed them.

What a long strange trip its been!

Abstract

This thesis presents an infrared spectral analysis of the high mass protostar W3 IRS5. A high resolution M band spectrum of W3 IRS5 was obtained from the CFHT with the Fourier Transform Spectrometer. The spectrum was measured using a Fortran program developed by the author. Four gas phase absorption components were detected in ^{12}CO with outflow velocities up to 38 km s^{-1}. Analysis of this absorption indicates gas temperatures up to 400 K with a temperature gradient possibly present. Source velocity ^{13}CO absorption, which was also detected, demonstrates that two separate gas clouds are present along the line of sight to W3 IRS5. Warm, neutral ^{13}CO gas has a temperature of 50 K whereas 300 AU from W3 IRS5, hot, 470 K, gas is detected. Absorption due to solid phase ^{12}CO is interpreted as originating in the warm, neutral gas some distance from the source. A rotationally supported accretion disk, which reprocesses starlight, may explain the hot gas close to the source.

The Examining Committee

Dr. George F. Mitchell
Professor of Astronomy
St. Mary's University
(Thesis Supervisor)

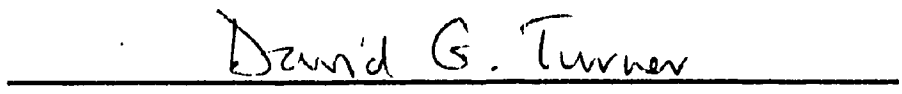

Dr. David G. Turner
Associate Professor of Astronomy
St. Mary's University

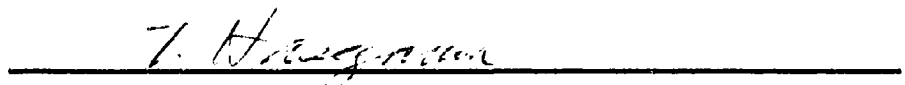

Dr. Tatsuhiko T. Hasegawa
Department of Astronomy
St. Mary's University

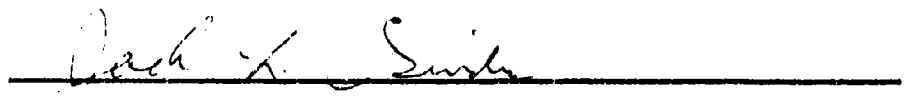

Dr. Jack L. Ginsburg
Professor of Chemistry
St. Mary's University

Table of Contents

Acknowledgements i

Abstract ii

The Examining Committee iii

List of Tables v

List of Figures vi

I Introduction 1

II Observations 21

III Reduction Process and Results 34

IV Discussion and Summary 62

References 78

Appendix A 82

Appendix B 96

Appendix C 97

Cirriculum Vitae 111

List of Tables

Table I — ^{12}CO V_{LSR} = −43.9 km s^{-1} Data 44

Table II — ^{12}CO $V_{LSR} = -54.4$ km s^{-1} Data 45

Table III — ^{12}CO $V_{LSR} = -72.6$ km s^{-1} Data 46

Table IV — ^{12}CO $V_{LSR} = -85.9$ km s^{-1} Data 47

Table V — ^{13}CO $V_{LSR} = -41.3$ km s^{-1} Data 48

Table VI — Summary of Velocities and Line Widths 49

Table VII — ^{13}CO Column Densities 51

Table VIII — ^{12}CO Column Densities at -54.4 km s^{-1} 54

Table IX — ^{12}CO Column Densities for High Velocity Lines 55

Table X — Summary of Column Densities and Temperatures 61

List of Figures

Figure 1	Large Scale Structure of W3	17
Figure 2	Principal Star Forming Sites in W3	18
Figure 3	Positions of Infrared Sources about W3 IRS5	19
Figure 4	Emission Wings Surrounding W3 IRS5	20
Figure 5	Bandpass Shape W3 IRS5	24
Figures 6a–d	Spectrum of W3 IRS5 and α Lyra	25
Figures 7a–b	Ratioed Spectrum of W3 IRS5 to α Lyra	29
Figure 8	Composite line profile of ^{12}CO	31
Figure 9	Six ^{12}CO Absorption Line Profiles	32
Figure 10	Bandpass Ratioed and Binned	33
Figure 11	Boltzmann Plot of ^{13}CO	56
Figure 12	Boltzmann Plot of ^{13}CO with best fit line	57
Figure 13	Boltzmann Plot of ^{12}CO $V_{LSR} = -54$ km s^{-1}	58
Figure 14	Boltzmann Plot of ^{12}CO High Velocity	59
Figure 15	Boltzmann Plot of ^{12}CO High Velocity with best fit line	60
Figure 16	Millimeter ^{12}CO Emission Profile	70
Figure 17	Schematic Diagram of Structure of W3 IRS5	72
Figure 18	Broadband (1–20 μm) Energy Distribution	75

I Introduction

In recent years, the process of star formation has been the subject of a great deal of observational and theoretical work. The results of early observational programs in the optical region of the spectrum demonstrated that high mass stars are located primarily along the galactic spiral arms and that low mass stars are distributed throughout the Galaxy. Optical studies are not able to contribute significantly to the understanding of the earliest stages of massive star formation because these stages take place deep within the dark clouds where the visual extinction is the largest. With the detection of molecules in the interstellar medium, the observational emphasis shifted from the visual to the infrared and microwave region of the spectrum. At these longer wavelengths, the dark clouds are more transparent and detailed studies of the very early stages of star formation could be initiated. Using the spectral features of the CO, CS, and NH_3 molecules, among others, many new and exciting phenomena associated with young stars have been discovered. These include: Herbig–Haro objects, high velocity maser sources and energetic mass outflow.

In a recent review, Shu, Adams and Lizano (1987) identified the major stages in the formation of stars. All stars form from dense cloud cores (embedded within the larger molecular cloud). These dense cloud cores, as well as their envelopes, are supported against dynamical collapse by turbulence, rotation, magnetic fields,

or other mechanisms. Eventually, they become unstable and dynamically collapse from the inside-out. Strong stellar winds are generated and push out at the weakest points in the cloud core (namely, the rotational poles). These outflowing winds are the likely precursors to bipolar outflows. The stellar winds gradually reverse the infall of matter and begin to disperse the cloud.

a. Characteristics of Star Forming Clouds

Observational studies in the infrared and microwave spectral regions have helped astronomers to more precisely determine the physical characteristics of star forming clouds. Zuckerman and Palmer (1974) established molecular clouds as the principal sites of star formation. Star forming clouds change from being predominantly atomic to being predominantly molecular when the density increases enough for self-shielding from ultraviolet radiation to occur (Hollenbach, Werner and Salpeter 1971). The most active sites of star formation are giant molecular clouds (GMCs) - with masses ranging from 10^5 to $3x10^6$ $M_\odot$ and their longest linear dimension exceeding ten parsecs (Solomon *et al.* 1979).

Recent high resolution observations of GMCs (using the spectral features of CO and NH_3) show the GMCs to possess considerable substructure. GMCs are complexes composed of smaller "clumps" with masses of 10^3 to 10^4 $M_\odot$, T $\sim$ 10 K, sizes from 2-5 parsecs, and densities of $10^{2.5}$ cm^{-3}. Smaller regions within the "clumps" contain gas of much higher density. These cloud cores are the predeces-

sors of protostars and can be mapped in H_2, HC_3N, NH_3, CS and in CO if the cloud cores are much warmer than their surroundings.

Mezger and Smith (1977) proposed that sites of high and low mass star formation may be spatially distinct. Solomon *et al.* (1985) classified molecular clouds into a warm and cold population. The cold clouds, with average temperatures less than 10 K, contain no stars earlier than late B spectral type, and are located throughout the galactic disk. The warm clouds, with average temperatures greater than 10 K, contain early type stars and are located along the galactic spiral arms. The findings of Solomon *et al.* are consistent with the original suggestion of Metzer and Smith.

Herbig (1962) suggested that the formation mechanism for high mass and low mass stars may be different. Solomon *et al.* (1985) noted that, whereas T Tauri (solar) type stars are observed scattered throughout molecular clouds, massive young stars often form near the boundary of molecular clouds. Since low mass stars are distributed throughout molecular clouds, low mass star formation can proceed directly from gravitational instabilities (i.e. no external trigger is required). High mass stars, on the other hand, preferentially form along the cloud periphery indicating the necessity for an external trigger to induce high mass star formation. The term induced star formation generally implies triggering by an external event such as the sudden compression of the interstellar medium (ISM)

by shock fronts, ionization fronts or stellar winds. It is tempting to associate the formation of high mass stars with the theory of externally induced star formation and the formation of low mass stars with the idea of spontaneous star formation. Unfortunately, this is probably too simplistic.

b. Cloud Support

Star formation rates in molecular clouds are considerably lower than expected indicating some cloud support is present. The minimum mass necessary for protostellar collapse is called the Jeans mass ($M_J \geq 1.795(RT/G)^{3/2}\rho^{-1/2}$, where ρ is the density and T is the temperature, and G and R have their usual meaning). Because the Jeans mass of clumps is much less than the actual clump mass, the clumps should be dynamically collapsing. The fact that most clumps are not observed to be dynamically collapsing indicates that they are supported against their self-gravity. Various mechanisms have been proposed to provide the clumps with enough energy to prevent their collapse, including rotation, turbulence, and magnetic fields.

Rotation as a means of cloud support is very unlikely by itself as the observed rotation speeds are much less than those needed for centrifugal pressure balance (Shu, Adams and Lizano 1987). Rotation may be important on a smaller scale, in the formation of cloud cores. As well, thermal support can be important for the envelopes surrounding the cloud cores. The envelopes, whose observed

temperatures are $T \sim 10$ K, can be understood in terms of a balance between cosmic ray heating and CO cooling. In the outer parts of the envelope, heating by photoelectrons from dust grains is an important additional contributor to the thermal energy content. While thermal energy may be sufficient to support the envelopes, it is unlikely to provide the support necessary for the rest of the cloud.

It is difficult to explain the presence of supersonic linewidths if they originate solely from turbulent dissipation of energy. The turbulent dissipation of energy is thought to be an important process in the evolution of molecular clouds. The sound speed for GMCs is typically 0.1 km s^{-1}. Since the observed CO linewidths are a factor of ten or more larger, supersonic motions are implied. These supersonic linewidths occur over the entire GMC (tens of parsecs). If the supersonic motions arise from the turbulent dissipation of energy, the flow velocities approach virial values. Supersonic velocities resulting from the turbulent dissipation of energy should be highly dissipative in the absence of magnetic fields. Supersonic turbulence should decay from shocks on timescales that are short compared to the lifetimes of GMCs. The dissipation of turbulence would lead to rapid collapse of the cloud and high star formation rates, much higher than those observed.

Turbulent support of small scale features in molecular clouds is much less likely than the support of the larger molecular cloud. The turbulent dissipation of energy per unit mass in a nonmagnetic medium will occur at the rate of v^3/l,

where v is the turbulent velocity and l is the characteristic scale size. Thus, turbulent support is more rapidly dissipated as the scale size decreases. In order for turbulence to provide mechanical support of molecular clouds, the turbulent velocity must be on the order of the virial speed, and l should be much less than the cloud size r. The turbulent dissipation timescale is $l/v \ll r/v$. Therefore, if the turbulent energy cannot be resupplied on a timescale faster than its dissipation rate, the cloud cannot be supported by turbulence alone.

Because magnetic fields are not as easily dissipated as turbulence, they should be considered as a major form of molecular cloud support. A magnetic flux Φ can support a cloud, provided the cloud mass does not exceed the critical value $M_{cr} = 0.13 \cdot \frac{\Phi}{\sqrt{G}} \approx 10^3 M_\odot (B/30\mu G)(R/2pc)^2$. Zeeman splitting of thermal OH allows measurement of the magnetic field strength component along the line of sight with typical values of $10^1 - 10^2 \mu G$ (e.g. Heiles 1987). Note that magnetic fields can support clouds only perpendicular to the magnetic field. The cloud can still collapse along the field lines. Observations of cloud clumps show they are not highly flattened along field lines. The support along B field lines may arise from nonlinear Alfven waves with $v_A \sim 1$ km s^{-1}. Because observations of cloud clumps show that they are not highly flattened, Alfvenic waves have been suggested to be the source of support perpendicular to the magnetic field lines.

c. Protostellar Core Formation

The gradual loss of magnetic and turbulent support in a molecular cloud core will eventually cause it to become unstable to gravitational collapse. Chandrasaker (1939) demonstrated that a slowly forming molecular cloud core that is not artificially separated from its surroundings by a boundary tends towards a density distribution of a singular isothermal sphere, namely $\rho = a^2/2\pi Gr^2$, where $a = (kT/m)^{1/2}$ is the isothermal sound speed. This agrees qualitatively with many observations of density distributions surrounding forming stars (Bally and Lada 1983, Keto *et al.* 1987). The density of an isothermal sphere tends to infinity at small r. Physically this implies a strong central mass concentration which should almost always cause spontaneous collapse to occur from the inside-out.

Accretion onto a growing protostar gradually shifts from the core to a "disk" or elongated structure. As long as it remains optically thin, the core of a high mass star collapses isothermally. The increase in the central density is halted only after the formation of an optically thick protostar ($M \sim 10^{-3} - 10^{-2}\ M_\odot$). The protostar then grows hydrostatically by accreting matter from infalling gas and dust. In any stably rotating cloud, the specific angular momentum must increase outward from the rotation axis. In the nonhomologous collapse of this type of cloud to form a star, the infall spreads out from the center at the local sound speed (Shu 1977). As the collapse proceeds, the maximum specific angular momentum of the infalling gas increases until the streamlines no longer intercept the core. From then on, the accretion flow slowly shifts from the core to a circumstellar disk around the

protostar (Yuan and Cassen 1984). The core accretion rate from the parent cloud decreases and the main accretion onto the protostar now occurs from a forming accretion disk in orbit around the star.

Since stars form in regions which possess large reservoirs of gas, it is unlikely that infall terminates from a lack of matter. A more likely explanation is that stellar winds eventually turn on, reverse the infall, and halt the accretion. Shu (1985) has suggested that the onset of deuterium burning in the core of the protostar may be responsible for driving the stellar winds. The energy released from burning deuterium will drive the star completely convective which, when coupled with differential rotation, may produce dynamo action and generate magnetic activity (Parker 1979). The released energy (which had been stored in rotation) may then power the intense stellar surface activity observed in YSOs. The resulting stellar winds reverse the infall, thereby defining the mass of the formed star at the point where it first becomes optically visible.

d. Molecular Outflow

In addition to their supersonic motions, molecular clouds also contain localized regions (cloud cores 0.1–3 parsecs in size) where a large fraction of the gas is moving at hypersonic velocities ($v \geq 100$ times the sound speed). In these regions the observed widths of molecular lines range from 10 to 100 km s^{-1}full width zero intensity (FWZI). These highly supersonic motions cannot be gravitationally (or

magnetically) bound to the local regions where they occur and therefore must be unbounded (Lada 1985).

The regions containing the hypersonic outflows are coincident with and usually centered on the positions of young stellar objects (YSOs) believed to be embedded in the cloud (see e.g. Claussen *et al.* 1984). The driving mechanism of the outflows is not clear, but, whatever the process, it is likely that strong stellar winds from the protostars will contribute. The winds may be isotropic when they leave the stellar surface, but since the accreting matter is mostly falling onto a disk, the point of least resistence for the stellar winds is the rotational poles. The winds break through at the poles and begin to sweep up matter as they move out. The swept-up matter will begin to reverse the infall, and a cone at the rotational poles will slowly widen towards the equator.

Observational evidence indicates that all YSOs pass through a stage of outflow, implying that outflow is a fundamental part of the star forming process (Lada 1985, Welch *et al.* 1985). The outflows are very energetic and exhibit a variety of associated phenomena such as Herbig Haro (HH) objects (Schwartz 1983), high velocity masers (Reid and Moran 1981), and "cometary" reflection nebulae (Strom *et al.* 1985). The molecular outflows are usually collimated and cold (Snell *et al.* 1980). Long narrow optical jets are sometimes present near low mass YSO's (Mundt and Fried 1983). The optical jets are often composed of linear chains of

HH objects which can be traced very close to the central stars, leaving no doubt as to their origin.

Molecular outflows tend to be spatially bipolar (Snell, Loren and Plambeck 1980), consisting of two spatially separate lobes of emission. One lobe contains mostly blue shifted gas and the other is dominated by redshifted gas. Lada (1985) surveyed 67 outflows and found 75% were bipolar, about 15% showed one lobe of emission (monopolar), about 8% were classified as isotropic, while the rest showed complex morphologies. Lada found that most flows were rather poorly collimated with a length to width ratio of about 2.4.

The large masses and energies of molecular outflows, along with their high frequency of occurrence, suggest they may be an important source of mechanical energy for molecular clouds. The masses of the outflows range from 0.1 to 100 $M_{\odot}$, in many cases equal to or larger than the mass of the central object. This seems to imply that the outflows are sweeping up mass as they move outwards rather than ejecting their initial mass. The kinetic energies of the outflows are very large, of order $10^{43} - 10^{47}$ ergs. The dynamical timescales of the flows are estimated to be between 10^3 and 10^5 yrs. The outflows could play a significant role in determining the structure and evolution of a GMC. As well, they may be able to generate the turbulence that maintains supersonic linewidths and supports the clouds from global gravitational collapse. This information collectively demon-

strates that molecular outflows play a significant role in both star formation and molecular cloud evolution.

c. Absorption Spectroscopy

The earliest stages in the birth of massive stars occur in dense, visually obscured molecular clouds. It has recently been discovered that these young stars return large amounts of material to their parent cloud. These outflows are composed of neutral, molecular material in which the highest velocity gas is sometimes quite warm. Most studies of molecular outflows have been undertaken using millimeter and radio techniques, which utilize large (arcminute) beams. These observations are unable to probe the inner regions surrounding the protostar where the outflows are thought to originate. This inner region, however, is of critical importance in understanding the outflows as a whole.

A relatively new and powerful way to observe molecular outflows is to use infrared absorption spectroscopy. This technique is powerful because it samples the inner regions of the molecular cloud with small (arcsecond) apertures. Absorption spectroscopy involves the measuring of absorption lines against the bright infrared continuum of the embedded protostar. This method probes a single line of sight to the continuum source and we expect the denser molecular material close to the source to show up most prominently. The velocities and profiles of the absorption lines, when compared with emission observations, can indicate the physical struc-

ture of the outflow and shed light on the acceleration mechanisms in the cloud. By observing molecular lines in differing excitation states, the temperature and density structure of the expanding gas can be determined.

A number of high resolution studies using infrared absorption spectroscopy in the 2–5 μm region have recently been undertaken on several embedded young stellar objects [e.g. the BN object (Scoville *et al.* 1983); GL2591 (Geballe and Wade 1985, Mitchell *et al.* 1988a); and M8E–IR (Mitchell *et al.* 1988b)]. Results show that despite the similarities in source masses and luminosities, significant differences are present in the outflow velocities, gas temperatures and cloud structures. For example, although the BN object and GL2591 both exhibit strong absorption at 3.1 μm and 9.7 μm with similar shaped continua (Willner *et al.* 1982), the BN object is a strong source of infrared recombination line emission (Brα, Brγ Scoville *et al.* 1983) while no lines are detected in GL2591 to one-tenth the intensity (Hall *et al.* 1978, Simon, Simon and Joyce 1979). Another important difference between the BN object and GL2591 concerns the shape of the infrared CO rotational lines. In GL2591, these lines are very strong and broad (full width greater than 150 km s^{-1}, Mitchell *et al.* 1988a), and were easily detected by Lacy *et al.* (1984) using an instrument with very low resolution (350 km s^{-1}). These same lines are very narrow in the BN object (Hall *et al.* 1978) and would be difficult to detect at low resolution.

Absorption spectroscopy has also been used to examine solid phase absorption due to CO and "XCN", which is thought to be NCO+, in several embedded protostars [in W33A (Lacy *et al.* 1984, Mitchell *et al.* 1988c); and in NGC7538/IRS9 (Lacy *et al.* 1984)]. The fundamental band of solid CO occurs at ~ 2140 cm^{-1} and for solid XCN at about 2165 cm^{-1} (Sandford *et al.* 1988). The solid absorption is thought to arise in cool, dense gas some distance from the source. By measuring the line strength, the column density of the solid absorption can be determined. If the column density of the gas phase CO can be determined for the same gas giving rise to the solid absorption, then the solid–to–gas phase ratio can be computed. This ratio is an important indicator of the depletion of carbon onto grain mantles. If significant quantities of carbon are locked up in grain mantles, then the gas phase chemistry of the cloud can be seriously affected. The first direct determination of the solid–to–gas phase ratio of CO was obtained by Mitchell *et al.* (1988c) along a single line of sight to W33A. Their results suggest that a small fraction (less than five percent) of CO is frozen on grains and that freezing out of carbon onto grain mantles will not significantly affect the gas phase chemistry.

Infrared absorption spectroscopy shows that, for some sources, the absorbing gas is moving at much higher velocities than the gas detected in emission at millimeter wavelengths. For example, the microwave CO emission lines of M8E–IR exhibit wings of total width of about 16 km s^{-1}(Bally and Lada 1983). An

M band absorption spectrum obtained by Mitchell *et al.* (1988b) evidenced several absorption components with velocities up to $\sim$ 150 km s^{-1}. The difference in these techniques is that millimeter observations detect extended line emission from both the front and the back of the source, whereas with absorption spectroscopy only the gas situated between the source and observer can be detected. This is why absorption spectroscopy is so useful in observing blueshifted outflows. The velocity of the source of the flow is given by the central velocity or peak of the millimeter emission line. The highest velocity gas may not be detected by millimeter observations because the filling factor of the high velocity gas will be small if it is close to the central source.

f. W3 Molecular Cloud

The W3–W4 region in the constellation Perseus comprises one of the most important and intensively studied star forming regions in the Galaxy. A number of interesting astrophysical processes have been identified on the largest and smallest scales. On the largest scale, Lada *et al.* (1978) mapped the millimeter-wave CO distribution over an area 1 degree in diameter. They argued that a prominent ridge of star–forming activity was the result of gravitational collapse occurring within material swept ahead of an expanding shock front. This front is part of the W4 HII region, centered about 30' southeast of W3. To the west of the star–forming ridge is a large, undisturbed, lower density molecular cloud in which little or no star-

forming activity is taking place (see Figure 1). Studies of the small scale structure have revealed three major centers of star formation within the star-forming ridge: W3, W3(OH), and AFGL333 (e.g. Lada *et al.* 1978; Thronson, Campbell and Hoffman 1980; Dickel 1980) see Figure 2. W3 is a complex of compact and diffuse HII regions, embedded stars, and OH and H_2O masers, all indicators of a high level of star-forming activity. The extremely luminous young stellar object, W3 IRS5, is embedded in the W3 complex. A diagram showing the relative positions of the masers and infrared sources in the core of W3 is shown in Figure 3.

W3 IRS5 displays a number of properties which indicate that it is probably a massive star in a pre–main–sequence stage. It is deeply embedded in a molecular cloud; broad, strong silicate absorption at 9.7 μm (Willner *et al.* 1982) implies a visual extinction in excess of 100 magnitudes. Jaffe *et al.* (1984) placed an upper limit to the visual extinction of 250 magnitudes. Weaker absorption due to water ice is present at 3.1 μm . Solid absorption of this type is usually associated with a cool, dense cloud some distance from the core. The total luminosity of W3 IRS5 is 6.9×10^5 $L_\odot$ (Mozurkewich *et al.* 1986) making it the most luminous young stellar object known. Microwave CO emission (J=1–0) lines of W3 IRS5 exhibit high velocity wings of total width at the 0.1 K level of 52 km s^{-1}(Bally and Lada 1983). The centroids of the red and blue wing millimeter emission are separated by 2", making W3 IRS5 the source of a bipolar outflow (Claussen *et al.* 1984) see Figure 4. W3 IRS5 is a resolved double source in the near infrared. The two

components are separated by 1" (Dyck and Howell 1982; Neugebauer *et al.* 1982) in the north-south direction.

This thesis presents the results of an investigation of the interstellar absorption lines in the direction of the luminous young protostar W3 IRS5. Our bandpass includes the (v=0-1) molecular bands of ^{12}CO and ^{13}CO , the Pfβ recombination line, and the fundamental bands due to solid phase ^{12}CO and ^{13}CO . From careful measurement of the intensities and profiles of the interstellar absorption lines present, we determine the gas temperature, density and velocity. We combine these results with those obtained by others (e.g. Bally and Lada 1983; Thronson, Lada, and Hewagama 1985), to present a simple, but significantly more detailed picture of the outflows originating from W3 IRS5.

Figure 1

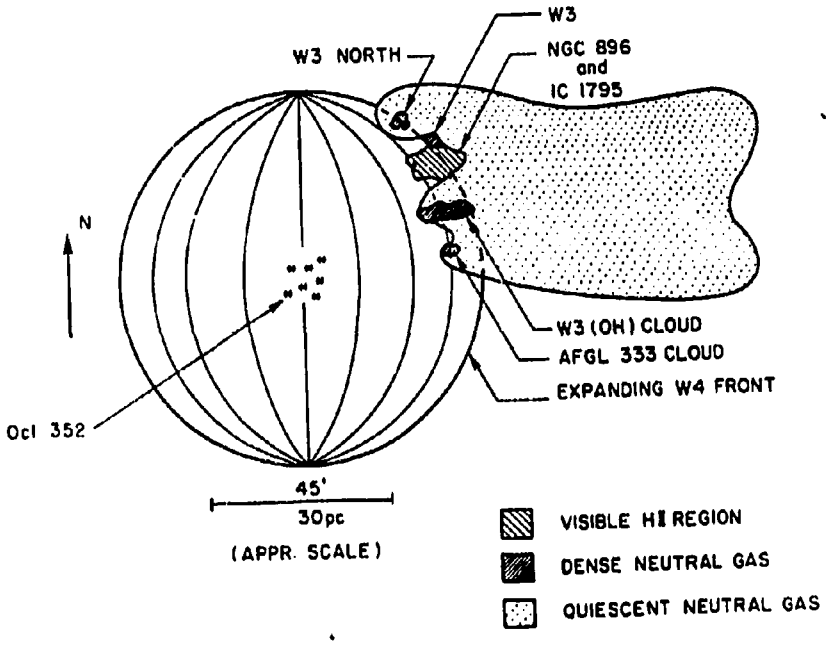

A schematic view of the W3/W4 complex (from Thronson, Lada, and Hewagama 1985). The source is viewed from Earth and is drawn roughly to scale. The location of the edge of the W3 HII region is shown only qualitatively and its front half is shown. W3 is therefore partially hidden.

Figure 2

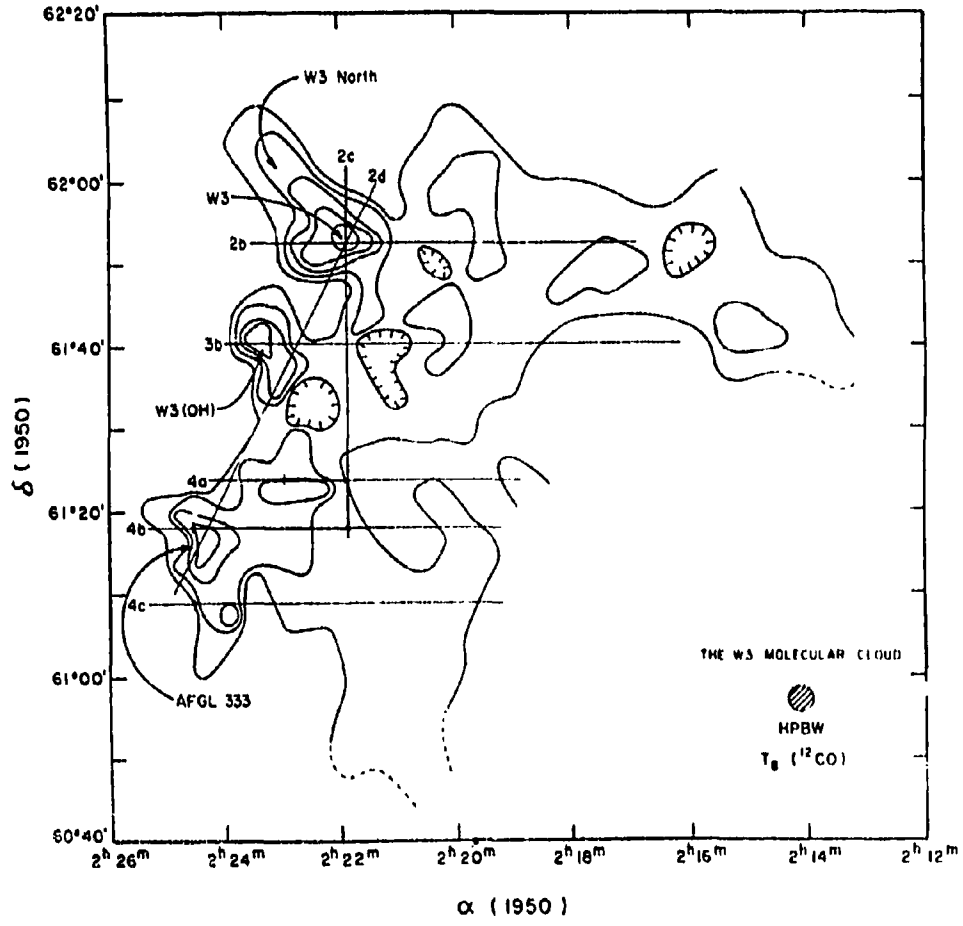

Distribution of the integrated ^{12}CO line strength in the W3/W4 complex (from Thronson, Lada, and Hewagama 1985). The major star-forming centers in the cloud are identified. W3 IRS5 is located in the core marked W3. The most intense activity stretches along a ridge (path 2d).

Figure 3

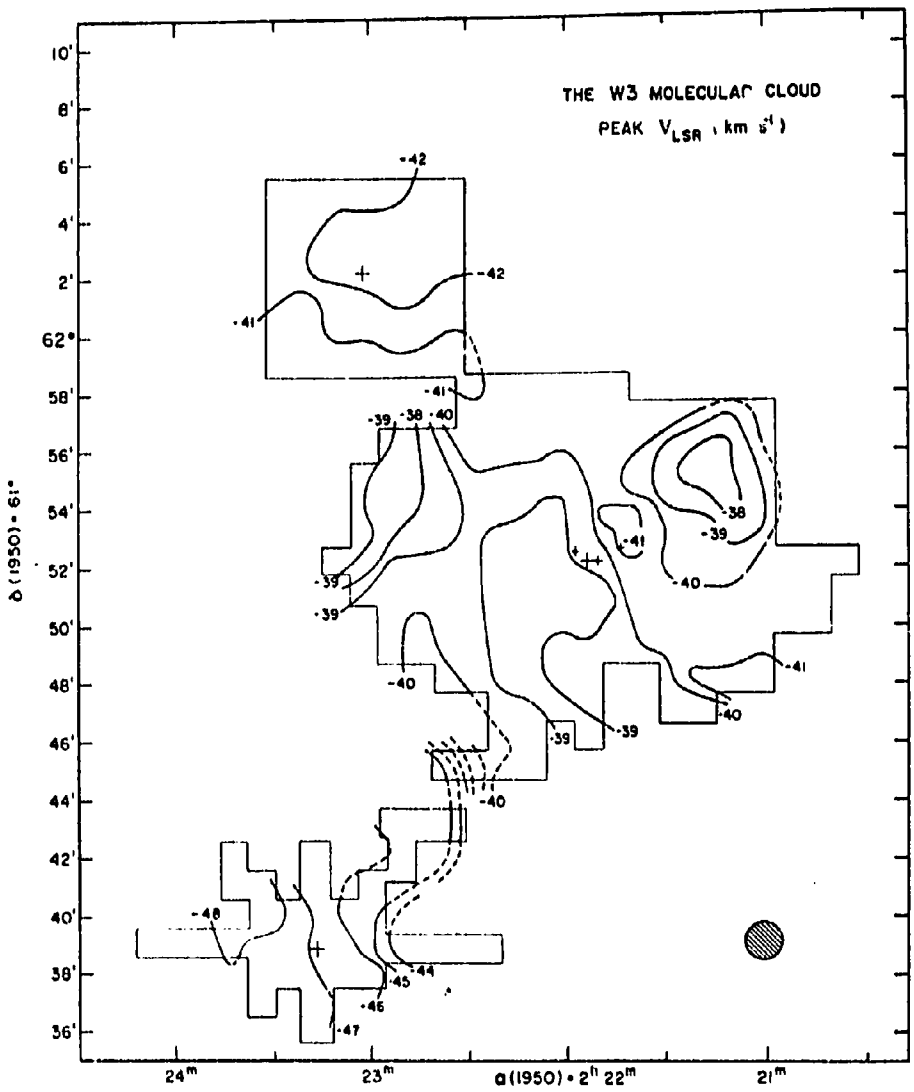

The LSR velocity of the emission line maxima in the W3 molecular cloud (from Thronson, Lada, and Hewagama 1985). The four central crosses are the positions of the mid-infrared point sources found by Wynn-Williams, Becklin, and Neugebauer (1972). From east to west they are IRS 2, IRS 5, IRS 3 and IRS4. The arms of the IRS 5 cross are each 15" long.

Figure 4

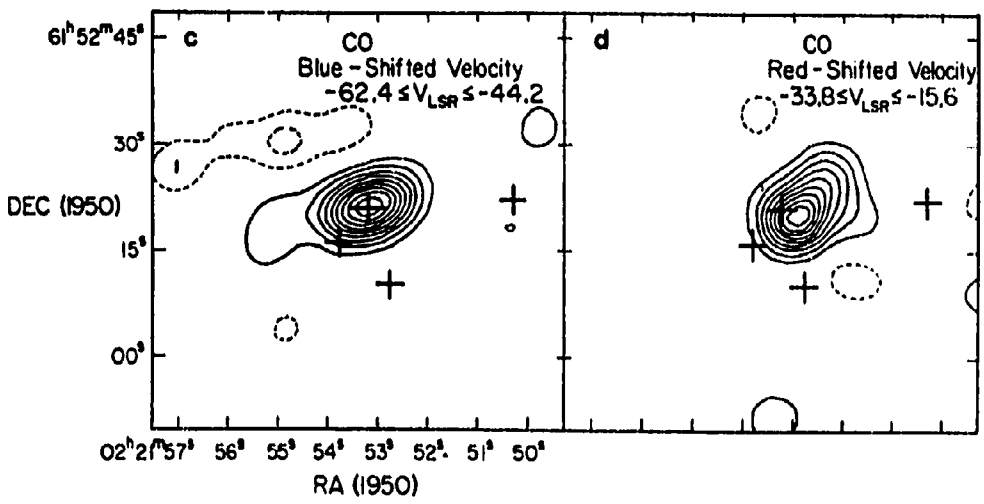

The crosses denote the four infrared sources, from left to right, IRS 6, IRS 5, IRS 7, IRS 3. The blueshifted emission is averaged over the velocity range -62.4 to -44.2 km s^{-1}. The contours are equally spaced with the lowest contour at 1.4 K. The redshifted emission is averaged over the velocity range -33.8 to -15.6 km s^{-1}. The contours are equally spaced with the lowest contour at 1.4 K. Diagram from Claussen *et al.* (1984).

II Observations

An infrared spectrum of W3 IRS5 was obtained by G.F. Mitchell on the 3.6m Canada-France-Hawaii Telescope on Mauna Kea, Hawaii, on the night of July 10-11, 1987, using the Fourier transform spectrometer (Maillard and Michel 1982) at the Cassegrain focus. The astronomical source was alternately placed in each of the two input apertures, 53 arcseconds apart, to subtract the residual background emission. There were cooled InSb detectors at each of the two outputs. An M band filter with a usable bandpass from 2080 cm^{-1} to 2180 cm^{-1} was employed. A spectral resolution of 0.0569 cm^{-1} was used; this corresponds to a velocity resolution of 8 km s^{-1}at 4.6 μm . A small entrance aperture of 2.5 arcseconds diameter was used to limit the thermal background. The total integration time was 81 minutes over a range of airmass centered at 1.55. The 2σ signal-to-noise (S/N) ratio in the spectrum is 7. A spectrum of α Lyr was obtained on the same night in order to provide a comparison spectrum for the removal of telluric absorption. The total integration time for the comparison spectrum was 65 minutes centered at an airmass of 1.35 with a final S/N ratio of 33.

The source spectrum, without correction for telluric absorption and without correction for the bandpass shape, is shown in Figure 5. Strong absorption lines approaching zero intensity are identified as the ^{12}CO source velocity lines. The complete source and comparison spectrum is shown in Figures 6a-d at a higher

dispersion. Source lines of ^{12}CO are labelled in Figures 6a–d, with the strongest absorption occurring at the source velocity. The ratioed spectrum of W3 IRS5 divided by α Lyr is shown in Figures 7a–b, with the lines of the fundamental vibrational band v=0–1 of ^{12}CO labelled above and of ^{13}CO labelled below the spectrum. There are a few lines of apparent emission visible in Figures 7a–b. These are not true emission features since they are not present in the high dispersion spectrum in Figures 6a–d. They result from the ratioing process when strong telluric lines are of different intensity in the source and comparison spectra.

Our spectrum shows absorption due to the fundamental bands of ^{12}CO and ^{13}CO . Lines of ^{12}CO show evidence of four discrete minima with the strongest absorption at the source velocity. As can be seen in Figure 8, the two strongest absorption features are separated by only 10 km $s^{-1}$with the result that they are partially blended. The two weaker ^{12}CO absorption features are also partially blended. Of the twenty-four ^{12}CO transitions detectable in the spectrum (R8–P15), 18 show the four velocity components clearly separated. The other transitions show a broadened and/or asymmetric absorption line. Portions of the spectrum near six of the ^{12}CO transitions are shown in Figure 9. In addition to the source ^{12}CO absorption, there is a moderately strong and narrow component due to ^{13}CO . A total of twenty lines, attributed to the rotational states R21–P4, have been identified. This ^{13}CO component has an average line width close to the 8 km s^{-1}resolution of the spectrogram and is probably unresolved. Since the

^{13}CO component does not suffer from line blending as the ^{12}CO absorption does, accurate column densities and temperatures can be determined.

As well, our spectrum shows absorption due to solid phase ^{12}CO and weak hydrogen recombination emission. In Figure 10, broad, weak absorption due to solid phase ^{12}CO is present, centered at ~ 2140 cm^{-1}. Solid ^{12}CO absorption was found by Lacy *et al.* (1984) in a low resolution scan of W3 IRS5. Our FWHM of ~ 4.3 cm^{-1} agrees with FW$(\tau/2) = 4.6$ cm^{-1} found by Lacy *et al.* (1984). Solid absorption due to the fundamental band of ^{13}CO occurs at ~ 2090 cm^{-1} which lies on the edge of our M band spectrum. No clear evidence of solid absorption from ^{13}CO can be seen in Figure 10 at this location. Weak emission centered at 2149.5 cm^{-1}, (which results from the Pfβ neutral hydrogen recombination line) can be seen in Figure 10.

The full width of the emission at zero intensity (FWZI) is about 300 km s^{-1}. The emission in Figure 10 is not convincing, but a recently obtained M band spectrum by G.F. Mitchell (private communication) also shows the same feature. This new spectrum can be considered definitive because its S/N ratio is about twice that presented here. Simon, Simon and Joyce (1979) originally detected Pfβ emission with a very low resolution (350 km s^{-1}) scan. However, they could not eliminate the possibility that it was an artifact of the reduction process. We provide verification of their initial discovery.

Figure 5

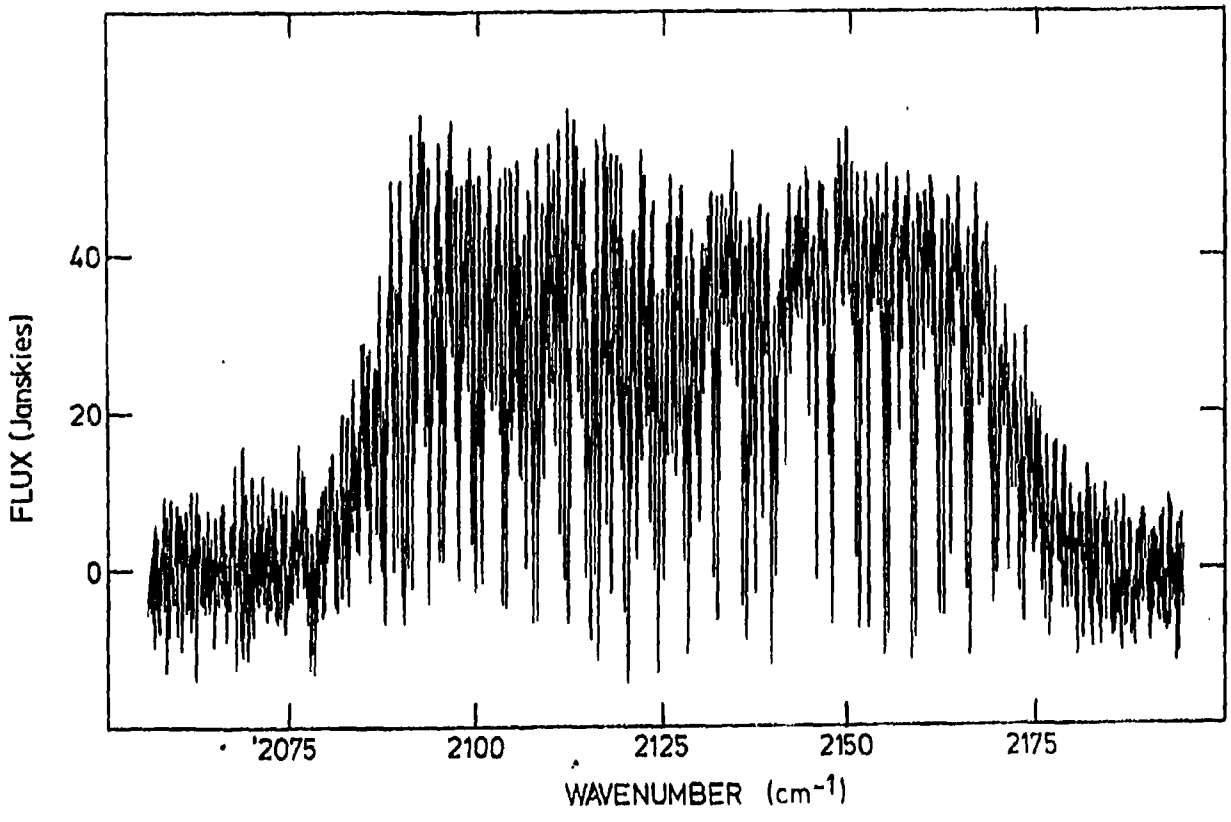

M band spectrum of W3 IRS5 without correction for telluric absorption or band-pass shape plotted from 2080 to 2180 wavenumbers.

Figure 6a

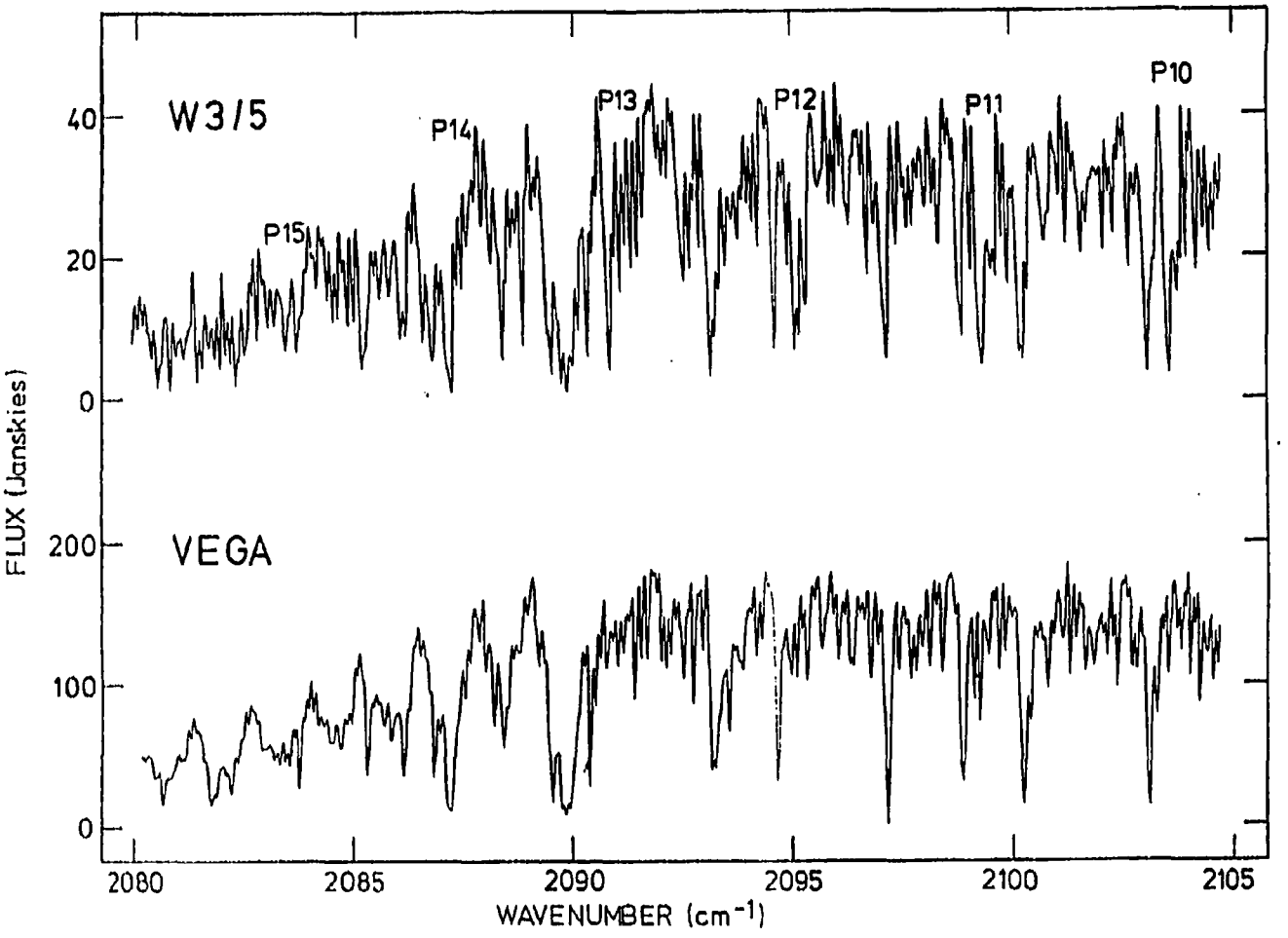

Spectra of W3 IRS5 and α Lyr without correction for telluric absorption or band-pass shape plotted from 2080 to 2105 wavenumbers.

Figure 6b

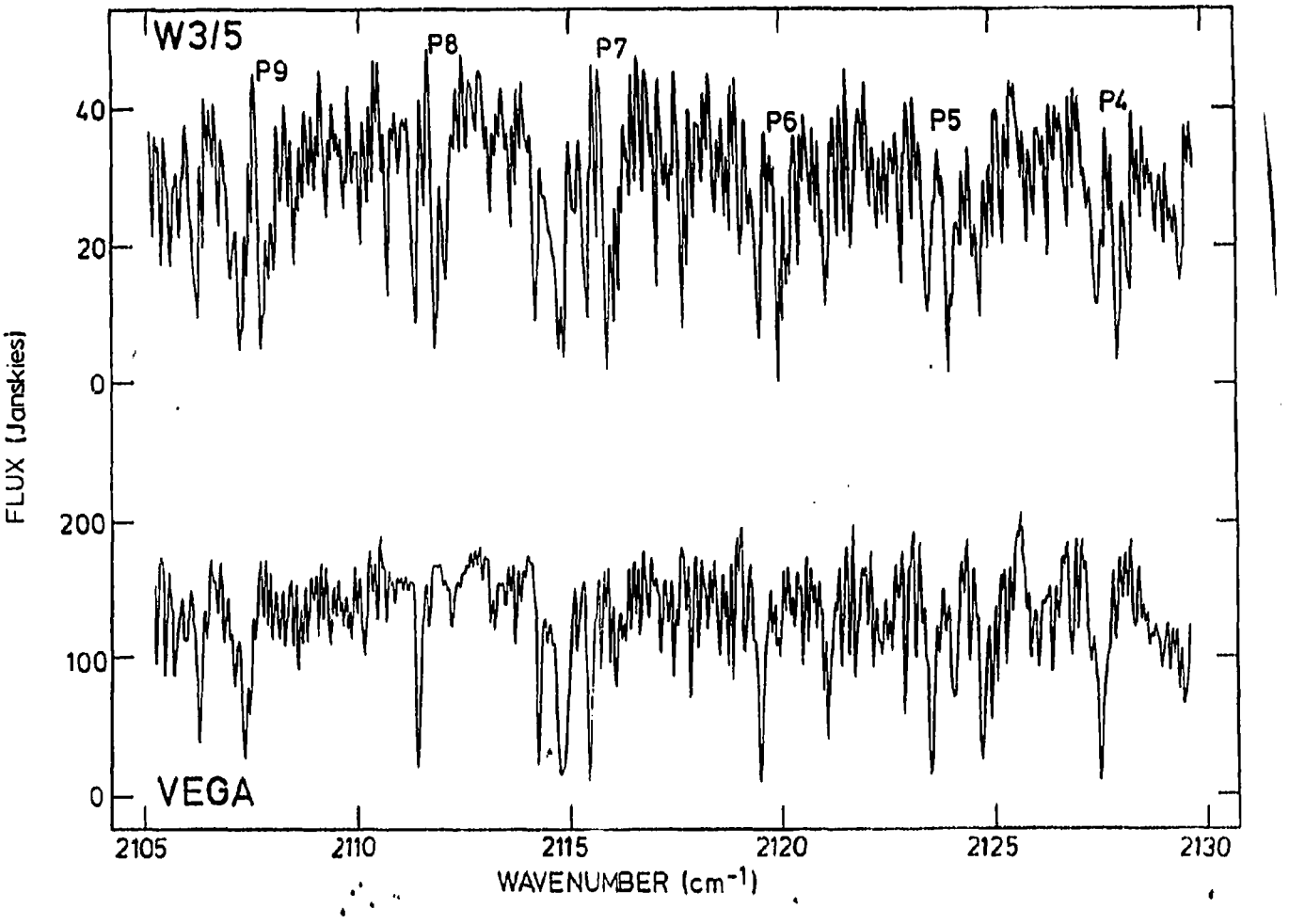

Spectra of W3 IRS5 and α Lyr without correction for telluric absorption or band-pass shape plotted from 2105 to 2130 wavenumbers.

Figure 6c

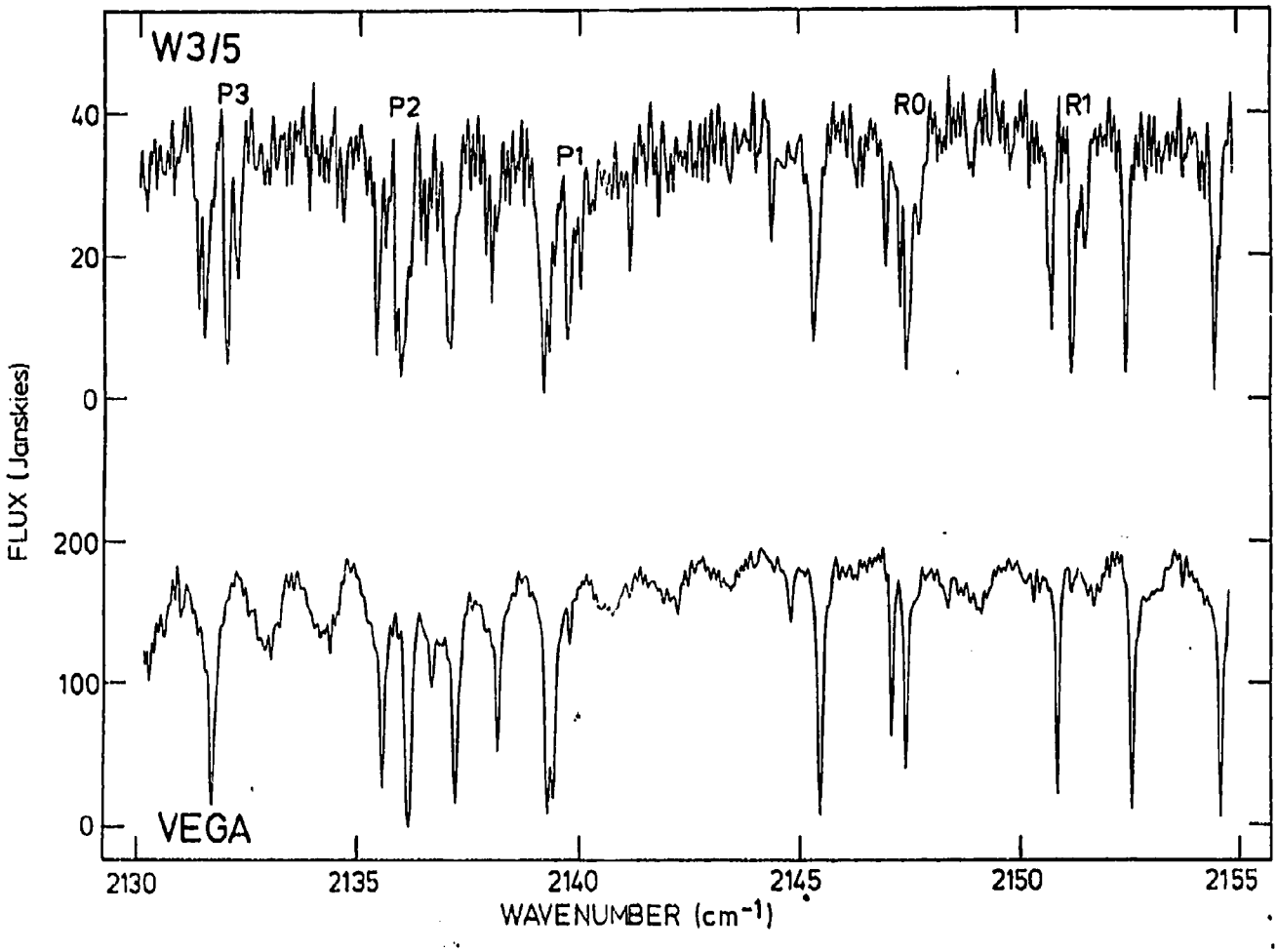

Spectra of W3 IRS5 and α Lyr without correction for telluric absorption or band-pass shape plotted from 2130 to 2155 wavenumbers.

Figure 6d

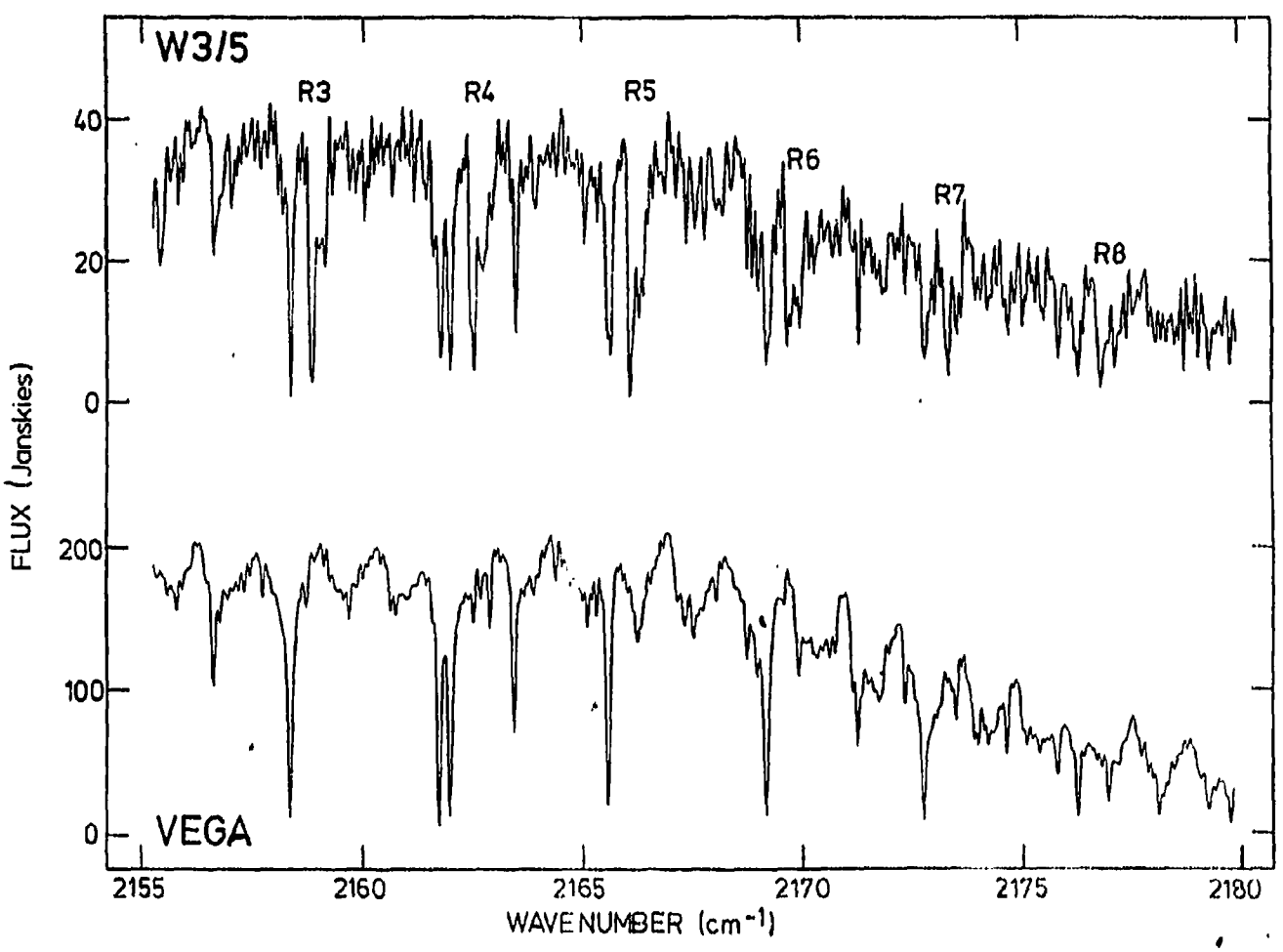

Spectra of W3 IRS5 and α Lyr without correction for telluric absorption or band-pass shape plotted from 2155 to 2180 wavenumbers.

Figure 7a

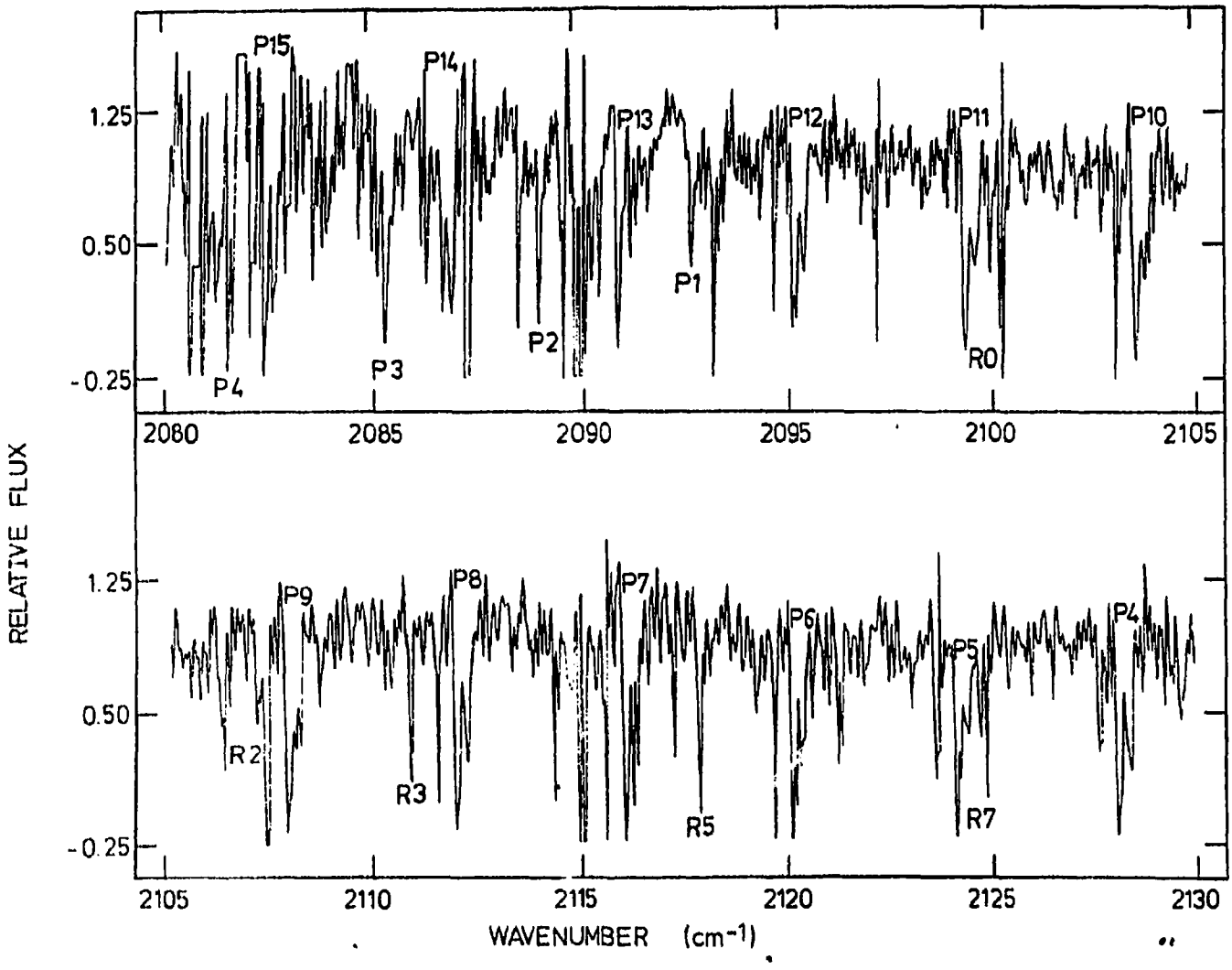

Ratioed spectrum of W3 IRS5 to α Lyr. Lines of rotation/vibration transitions of ^{12}CO are labelled above the spectrum, and ^{13}CO below the spectrum.

Figure 7b

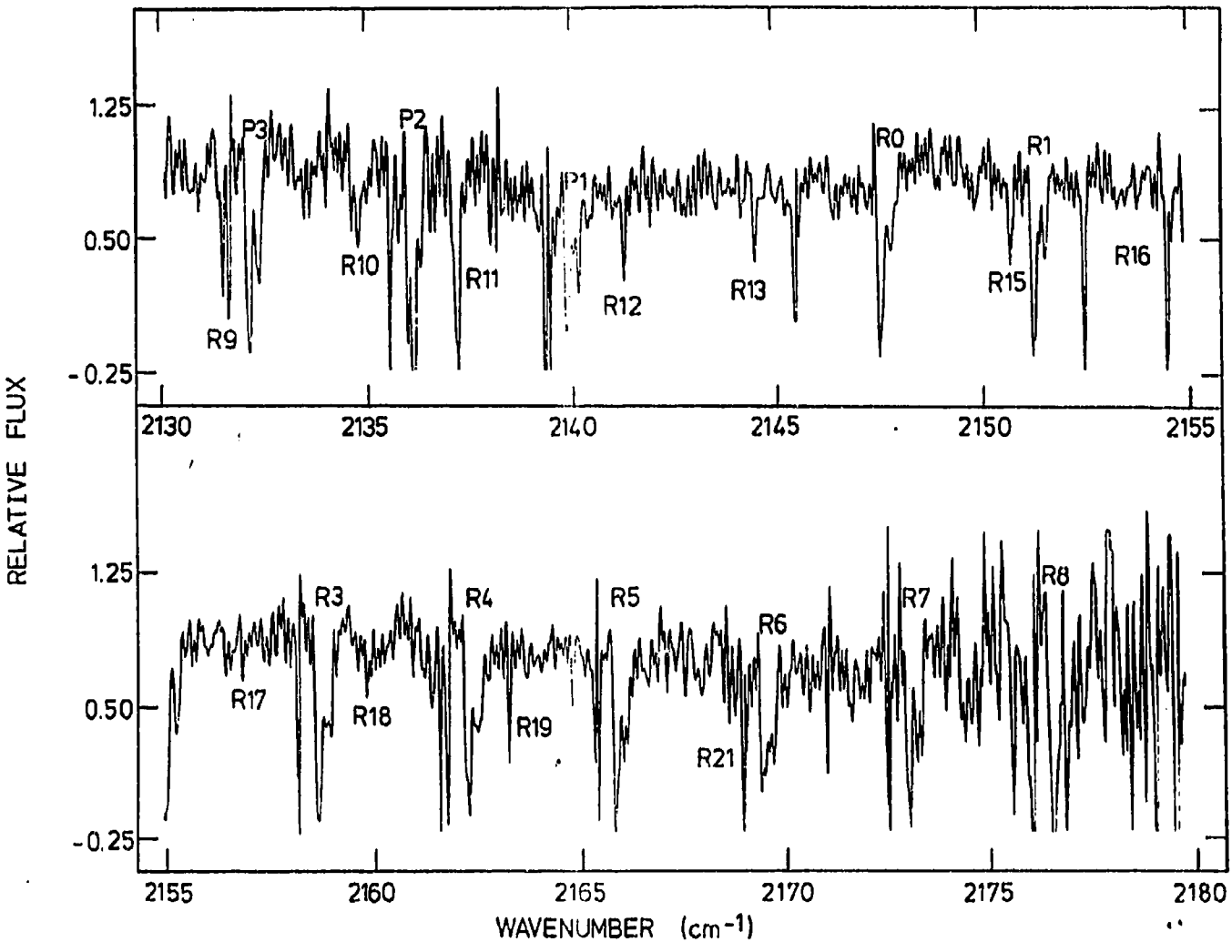

Ratioed spectrum of W3 IRS5 to α Lyr. Lines of rotation/vibration transitions of ^{12}CO are labelled above the spectrum, and ^{13}CO below the spectrum.

Figure 8

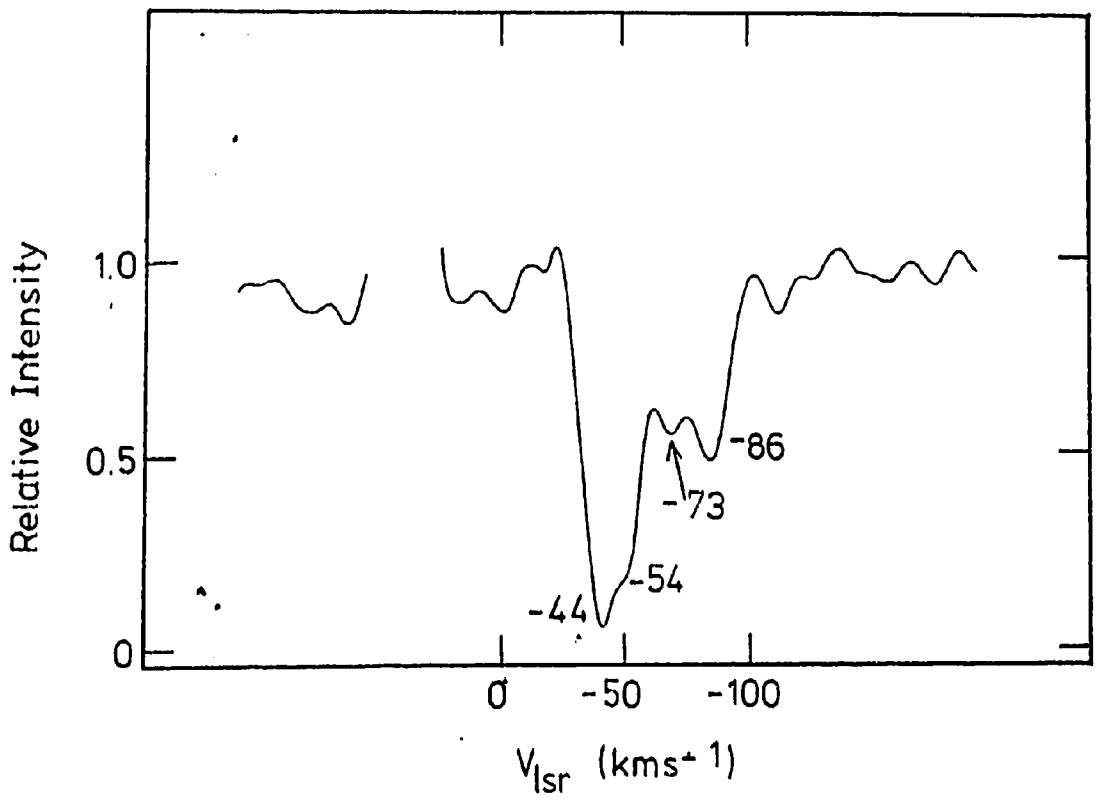

Composite profile formed from 10 lines of ^{12}CO . Four discrete absorption components are visible.

Figure 9

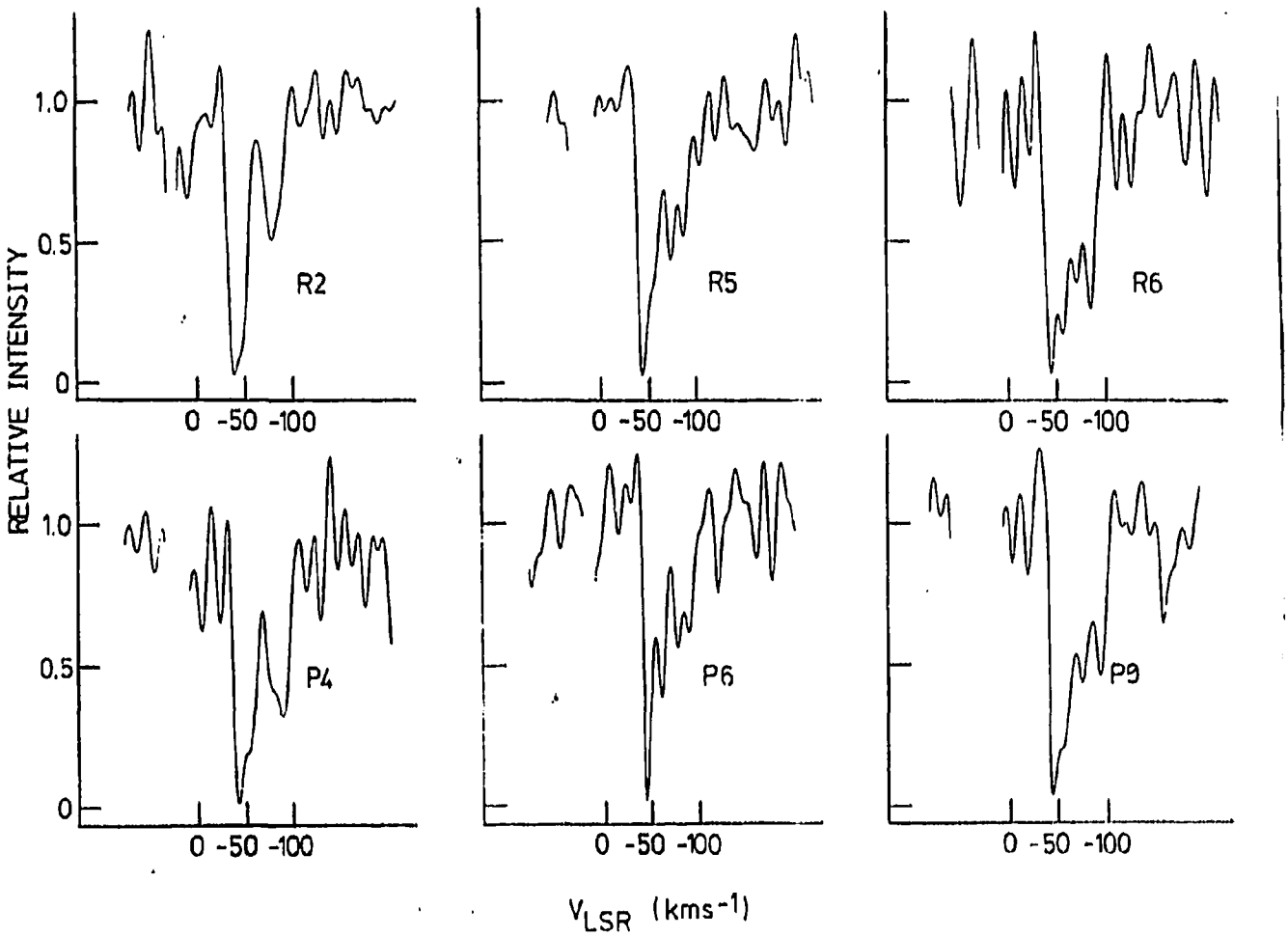

Absorption profiles of six ^{12}CO lines. The four absorption components are identifiable in each profile. Two broad features with two components comprising each are clearly evident. Compare with the composite line profile in Figure 8.

Figure 10

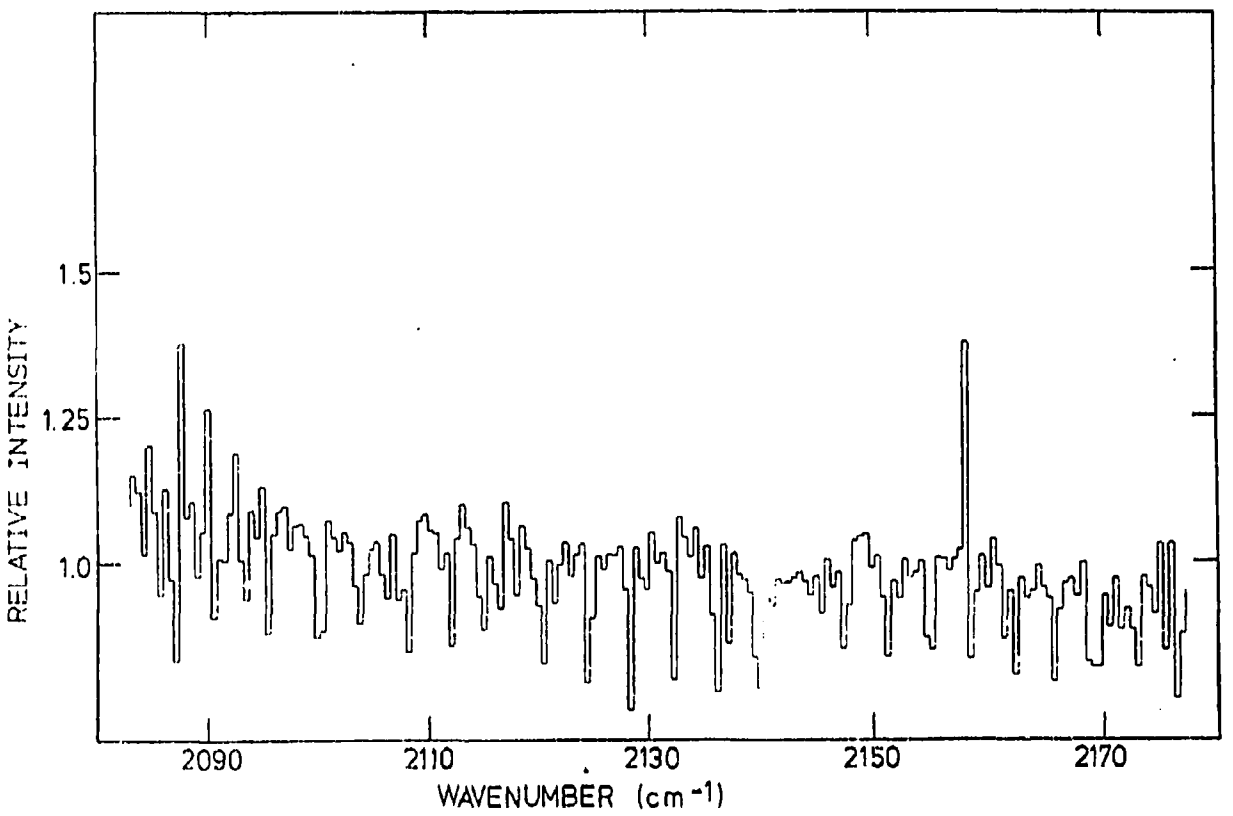

Bandpass from 2080 to 2180 wavenumbers. It has been ratioed and binned into 200 bins to highlight broad weak absorption of ^{12}CO at 2140 cm^{-1} and possible Pfβ emission at 2150 cm^{-1}.

III Reduction Procedure

The initial analysis of our M band spectrum identified absorption lines due to ^{12}CO , ^{13}CO , solid ^{12}CO absorption and a Pfβ recombination emission line. The measurement of the positions, strengths, and widths of these features was accomplished with the help of a computer program written specifically for this purpose. This computer program aided the reduction process by ensuring that the data were consistently handled and measured as accurately as could reasonably be achieved. Appendix A provides an overview of the computer program and Appendix B provides flow charts to guide the uninitiated in its use. Appendix C provides a list of subroutines and a brief description of each one.

The spectrum was measured using the computer program RPFTS written as part of this thesis. The program incorporates a number of assumptions into its decision making of which those listed below are the most critical. For example, the program assumes the spectrum data files used as input conform to the file format as detailed in Appendix A, of the Fourier Transform Spectrometer Data Reduction Program Users Guide (Link 1987). As well, when the user is measuring with the crosshairs, the position of the crosshair thread is included in the integration over the spectral line when computing the equivalent width. The program also assumes that the horizontal line displayed on the screen is the location of the continuum. Therefore, the determination of the full width at half maximum (FWHM) (which

involves computing the half maximum point) is taken to be halfway from this horizontal line (representing the continuum) to the absorption minimum.

The general reduction procedure went as follows. The source and comparison spectra were both displayed, centered about the desired line. In order to match the continua of the two spectra, the source spectrum was offset in intensity relative to the comparison. Repeated shifts in the source intensity allowed the user to effectively match the continua of the two spectra. The ratioed spectrum was then formed by dividing W3 IRS5 by α Lyr and was displayed centered about the desired line. A horizontal line representing the continuum, with a value of unity, was also displayed. With the continuum of the ratioed spectra matched to the horizontal line, the features position, width, and strength were measured using the options "L", "F', and "E", respectively. The option "L" lists the position of the vertical crosshair in wavenumbers, while option "F" provides an estimate of the full width at half maximum (FWHM). In option "E", the program integrates over the spectral line, providing a measure of the equivalent width and also giving an estimate of the full width at zero intensity (FWZI).

The measured positions (in wavenumbers) of the absorption lines were used to calculate the observed velocity of the feature in km s^{-1}. The rest positions of the ^{12}CO and ^{13}CO lines (in cm^{-1}) were taken from Kirby-Docken and Liu (1978). The Doppler equation is $\Delta\omega/\omega_0 = v_{obs}/c$, where ω_0 is the rest wavenumber, $\Delta\omega$

is the difference between the rest and observed position (in wavenumbers), and v_{obs} is the radial velocity of the object. The velocity of the earth relative to the object changes as the earth moves in its orbit, so common practice is to correct the object's velocity to the solar system barycenter. Following this, most researchers correct the barycentric velocity for the sun's motion relative to the Local Standard of Rest (LSR). This latter correction is not well-established, and the common practice for studies at radio and microwave frequencies is to approximate it with the Kinematical (as opposed to the more valid Dynamical) LSR correction. This is the case in this thesis as well, and a correction factor (including barycentric correction) of $\Delta V_{LSR} = +20.6$ km s^{-1} was added to all velocities to compute velocities relative to the LSR. Note that all velocities quoted below are LSR velocities unless otherwise stated.

The local standard of rest velocities of the four ^{12}CO absorption components are found to be $V_{LSR} = -43.9 \pm 2.7$, -54.4 ± 3.5, -72.6 ± 3.9, and -85.7 ± 2.9 km s^{-1}(1 σ errors quoted). The LSR velocities and errors were computed by taking the average of all the lines present at that velocity. The velocity of the -43.9 km s^{-1}component coincides, within 1 σ, with the central velocity of the ^{12}CO (J=1–0) emission line (-41.3 km s^{-1}Bally and Lada 1983). Therefore, we identify the -43.9 km s^{-1}component with gas at the velocity of the central object. The -54.4, -72.6, and -85.7 km s^{-1}components can then be interpreted as gas flowing from W3 IRS5 with a velocity of 13.1, 31.3, and 44.4 km s^{-1}, respectively. The

LSR velocity of the ^{13}CO gas is $V_{LSR} = -41.3 \pm 2.4$ km s^{-1}. This LSR velocity agrees with that of the ^{12}CO absorption and can be identified with gas at the velocity of the central object.

The line positions were measured using the program RPFTS (option "L"). As Figure 8 demonstrates, the ^{12}CO absorption consists of two broad features with two discrete minima on each broad feature. The stronger broad feature contains the source velocity component (at -44 km s^{-1}) and a weaker feature at -54 km s^{-1}. The weaker broad feature, which we will refer to as the high velocity feature, is composed of two components at -73 and -86 km s^{-1}. The lines at -73 and -86 km s^{-1} were nearly equal in strength and usually showed discrete minima, which were taken to be the line centers. The broad low velocity feature is dominated by the source velocity absorption at -44 km s^{-1}. The ^{12}CO source velocity minimum is not sharp, but is present in each line in the series, whereas the feature at -54 km s^{-1} resembles a bump on the blue wing of the source velocity feature (see Figure 9). The measurement of the line position for the source velocity gas was straightforward, but the position of the line at -54 km s^{-1} showed no definite minimum in most cases, so the center of the rounded bump was taken to be the line center. A total of 18 absorption lines at -54 km s^{-1} were detected and measured at similar velocities, so the feature is unlikely to be noise. The ^{13}CO source velocity lines have well defined minima; thus they presented no problems in measuring their line centers.

Due to the nature of the ^{12}CO absorption, it is not possible to know whether the broad features result from the superposition of discrete lines or from the continuous outflow of material leading to asymmetric, blueshifted lines. The ^{13}CO lines are narrow and show no evidence of asymmetry or broadening. We assume the ^{12}CO features at -54, -73, and -86 km s^{-1} to be discrete absorption lines.

The FWHM are not the intrinsic line widths. Being artificially broadened by the instrumental profile, the FWHM must be corrected using the relation

$$(\Delta v_{1/2})^2 \approx (\Delta v_{obs})^2 - (\Delta v_{inst})^2,$$

where $\Delta v_{1/2}$ is the intrinsic line width, Δv_{obs} is the FWHM and Δv_{inst} is the instrumental resolution. The instrumental width can be computed by solving for v in the Doppler equation, with ω_0 equal to the wavenumber at the pass-band center (2130 cm^{-1}) and $\Delta\omega$ equal to the spectral resolution in wavenumbers (0.0569 cm^{-1}). The instrumental width of our spectrum is 8 km s^{-1}.

The line widths were measured using the program RPFTS (option "F"). However, the ^{12}CO widths are unreliable because they are blended and suffer degradation from a low spectrum S/N ratio. For some lines, the FWHM is not an accurate measure of the true line width. In this case, the program also computes values for the two half widths at half maximum. As well, the program takes twice the narrower of these as a second estimate of the FWHM. The program displays both the FWHM and this estimated FWHM (EFWHM) each time option "F"

is called. Comparison of the FWHM and EFWHM of the unblended ^{13}CO lines showed they were in close agreement.

The FWHM of the ^{12}CO lines were difficult to determine because each line had only one-half of a line profile to measure. This is evidenced in Figure 9. For these lines with only one-half a line profile, the EFWHM was a better measure of the line width. The ^{13}CO lines were fairly symmetric and unblended so they were easy to measure.

The minimum detectable equivalent width is the equivalent width of the noise in the spectrum. It is essential to estimate this parameter in order to establish a limit for the strength of "real" features. Features with strengths less than the minimum detectable equivalent width cannot be considered "detections". The minimum detectable equivalent width is computed by taking the spectral resolution (0.0569 cm^{-1}) and dividing it by the S/N ratio (in our spectrum this is about 7). Therefore, features with line strengths less than $0.0569/7 = 0.008$ cm^{-1} are in the noise and should not be used.

The line strengths were measured using the program RPFTS (option "E"). When measuring the equivalent width, the program displayed vertical threads on the terminal. These threads were placed on either side of the line to be measured. The program integrates over the line, including the position of both vertical threads, to compute the line strength. In order to provide a means of estimating

the measuring uncertainty, the equivalent width of three lines were measured five times consecutively. The repeated measurements agreed to better than 10 percent. The program also estimates the full width of the line at the continuum (FWZI). As well, the program is capable of measuring single narrow lines (absorption or emission) and broad features such as absorption due to solid CO.

In order to measure the equivalent width of the ^{12}CO absorption, it was necessary to split the two broad features into two sections, taking their relative line strengths into account. The split was always made so that the sum of the equivalent width of the two lines equaled the equivalent width of the entire absorption feature. Splitting the broad feature into two lines was most difficult for the broad, low velocity feature containing the source velocity gas. Because this line was so much stronger than the line at -54 km s^{-1}, the feature was split with the break very close to the minimum of the weaker line. It was much easier to split the broad, high velocity feature because the lines were more nearly equal in strength. For the lines on the broad, high velocity feature, the split occurred near the middle of the two minima and slightly closer to the weaker minimum, so the equivalent width was larger for the stronger line.

Two difficulties arose when measuring spectral lines. The first was due to a sinusoidal modulation of the continuum, known as channeling, which is present in all CFHT Fourier Transform spectra. The channeling cannot be removed reliably

and causes difficulty in fitting the continua of the source and standard. The second difficulty resulted from strong telluric absorption lines in the source spectrum which were not completely removed in the ratioing process. The strong telluric absorption causes artifical emission lines to appear in the ratioed spectrum. These can be shown to be artifacts of the ratioing process by close examination of both spectra individually, looking for the presence of real emission lines. The spikes are not a problem unless they interfere with the measurement of the source absorption lines. If the telluric lines in the comparison spectrum were scaled so that they were of the same intensity as the telluric lines in the source spectrum, the telluric lines would be effectively removed from the ratioed spectrum. The difficulty with this approach is that the S/N ratio of the comparison spectrum would be severely degraded and the noise level in the ratioed spectrum would increase in kind.

It should be pointed out that, when the spectra are ratioed, individual line shapes can change as the source spectrum is vertically/horizontally shifted with respect to the standard. The change in the line shape is generally small unless strong telluric absorption is present. If source lines are coincident with strong telluric absorption, the measured position, line strength and width will be somewhat less reliable.

The determination of the lines' position, width, and strength are estimated by very simple techniques. Computer programs are available to take spectra,

deconvolve the instrumental profile and fit gaussians to the features. Our spectra are not in a data format that is compatible with these elaborate programs. While it is much more reliable to use the method of artifical line blends to measure the lines, it was beyond the scope of this thesis to attempt such a project. The simplistic approach taken here is ideally suited for unblended lines. The measurement of strongly blended features shows the weakness of this simplified approach.

The most significant contribution to error in the data results from the subjective interpretation of the user. The positions of the line centers are fairly easy to estimate consistently. The fitting of the continuum, however, is arbitrary; only by careful consideration of the spectrum and with considerable practise can this be accurately accomplished. If the continuum is poorly fit, the line positions measured will not be seriously affected, but, the line width, and particularly the line strength, will suffer appreciably. Thread positioning by the user is also subjective and is another important source of error. Placement of the threads, when measuring the line strength, requires the user to "know" where the line begins and ends. This clearly is not the case.

It is also important to calibrate the program to be sure the output is accurate. A recent graduate of Saint Mary's University measured the line positions, widths and strengths of a spectrum of GL2591 by hand. Afterward, he was shown how to use the program RPFTS and was asked to remeasure those same quan-

tites. Although we have no quantitative results, we found no significant differences between the values produced by the program and the values measured by hand.

a. Results

The data taken with the computer program are presented in Tables one through five. Tables I , II , III , and IV correspond to the four ^{12}CO components in order of increasing LSR velocity. Table V contains the ^{13}CO data. The rest positions for the ^{12}CO lines (from Kirby-Docken and Liu 1978) are tabulated once in column three of Table I . The velocity shifts in Tables I , II , III , and IV are computed using these rest positions. The rest positions for the ^{13}CO are in column three of Table V .

Table VI summarizes the line width and velocity data for the four components of ^{12}CO and the source velocity feature of ^{13}CO . The number of lines measured in the series is listed in column two. The average LSR velocity of each component with its 1 σ error is listed in column three. The average FWHM with 1 σ error is listed in column four. The intrinsic line width computed from the average FWHM in column four is presented in column five.

The calculation of the column density from the equivalent width is dependent on several factors. The optical depth in the line is the most important of these. If the line is saturated, (i.e. the line core reaches zero intensity) then the optical

Table I

^{12}CO Absorption at $V_{LSR} = -43.9$ km s^{-1}

Line	Observed ω (cm^{-1})	Rest ω (cm^{-1})	Velocity Shift (km s^{-1})	FWHM (km s^{-1})	Equivalent Width (cm^{-1})
R0	2147.537	2147.081	−63.7	13.66	0.06352
P1	2139.880	2139.426	−63.7	13.16	0.04231
R1	2151.310	2150.856	−63.3	14.72	0.10300
P2	2135.978	2135.546	−60.7	10.98	0.05483
R2	2155.055	2154.596	−63.9	15.79	0.06731
P3	2132.123	2131.632	−69.1	19.26	0.11550
R3	2158.787	2158.300	−67.7	20.65	0.10940
P4	2128.119	2127.683	−61.5	13.23	0.07088
R4	2162.420	2161.968	−62.7	14.65	0.04391
P5	2124.135	2123.699	−61.5	11.04	0.05677
R5	2166.061	2165.601	−63.7	14.08	0.06625
P6	2120.124	2119.681	−62.7	9.96	0.06323
R6	2169.637	2169.198	−60.7	11.35	0.05134
P7	2116.074	2115.629	−63.1	12.75	0.06162
R7	2173.224	2172.759	−64.2	14.03	0.04500
P8	2111.988	2111.543	−63.2	12.77	0.06533
R8	2176.773	2176.284	−67.4	15.63	0.05397
P9	2107.875	2107.423	−64.3	13.91	0.06727
P10	2103.764	2103.270	−70.4	18.96	0.09448
P11	2099.533	2099.083	−64.4	20.11	0.09366
P12	2095.301	2094.862	−62.7	9.51	0.04556
P13	2091.082	2090.609	−67.9	15.15	0.06909
P14	2086.799	2086.322	−68.6	12.93	0.04319
P15	2082.459	2082.002	−65.9	9.01	0.02444

depth in the line is large (i.e. it is optically thick; $\tau \gg 1$). When this occurs, the calculation of the column density from the equivalent width is not straightforward and a curve of growth analysis must be employed. If the line is optically thin, with $\tau \ll 1$, the calculation of the column density per rotational sublevel from the

Table II

^{12}CO Absorption at $V_{LSR} = -54.4$ km s^{-1}

Line	Observed ω (cm^{-1})	Velocity Shift (km s^{-1})	FWHM (km s^{-1})	Equivalent Width (cm^{-1})
R0	2147.607	−73.5	18.02	0.03666
P2	2136.080	−74.9	7.69	0.01883
R2	2155.108	−71.3	15.78	0.04573
P4	2128.205	−73.6	15.43	0.04895
R4	2162.485	−71.7	13.56	0.05192
P5	2124.246	−77.2	48.04	0.02393
R5	2166.132	−73.5	15.16	0.03067
P6	2120.224	−76.9	11.62	0.04758
R6	2169.725	−72.9	36.22	0.04052
P7	2116.140	−72.5	13.30	0.03635
R7	2173.286	−72.7	13.49	0.05419
P8	2111.058	−73.2	16.11	0.04841
R8	2176.873	−81.2	12.93	0.01559
P9	2107.943	−74.0	35.61	0.03810
R9	2180.297	−72.2	10.22	0.03399
P12	2095.395	−76.2	14.54	0.05209
P13	2091.196	−84.2	8.97	0.00997
P15	2082.543	−78.0	9.58	0.02302

equivalent width can be computed using $W_\omega = (\pi e^2/m_e c^2) N_J f_J$ (Spitzer, 1978). Inserting the values for the constants yields $N_J = W_\omega/(8.85 \times 10^{-13} f_J)$ where f_J is the transition probability of the J^{th} state (Kirby-Docken and Liu, 1978) and W_ω is the equivalent width in units of cm^{-1}. The column density N_J, defined as the number of molecules per unit area along the line of sight, has units of cm^{-2}.

If the absorbing gas is in local thermodynamic equilibrium (LTE), the column

Table III

^{12}CO Absorption at $V_{LSR} = -72.6$ km s^{-1}

Line	Observed ω (cm^{-1})	Velocity Shift (km s^{-1})	FWHM (km s^{-1})	Equivalent Width (cm^{-1})
P1	2140.062	−89.2	48.78	0.01743
R1	2151.477	−86.5	11.99	0.02024
P2	2136.220	−94.7	7.69	0.04450
P3	2132.295	−93.3	18.70	0.03556
R3	2158.946	−89.7	47.81	0.04136
P4	2128.359	−95.4	15.98	0.04082
R4	2162.688	−99.8	31.43	0.04372
P5	2124.373	−95.2	40.31	0.02982
R5	2166.259	−91.1	37.36	0.02845
P6	2120.343	−93.6	34.85	0.04054
R6	2169.821	−86.1	45.41	0.02821
P7	2116.261	−89.7	9.42	0.03616
R7	2173.458	−96.5	19.97	0.03823
P9	2108.066	−91.5	47.30	0.03736
P10	2103.943	−96.0	37.91	0.03688
P11	2099.781	−99.8	28.49	0.05489
P12	2095.514	−93.2	41.42	0.01338
P14	2086.965	−92.4	12.37	0.02870
P15	2082.670	−96.2	11.83	0.03024

density is related to the rotational temperature (T) by the equation

$$N_J = N_T \frac{g_J\, e^{-E_J/kT}}{\mu(T)},$$

where N_T is the total column density of molecules in the ground vibrational state, E_J is the rotational energy of the J^{th} state, g_J is the statistical weight of the J^{th} state, $\mu(T)$ is the appropriate partition function and k is Boltzmann's constant. For diatomic molecules, $g_J = 2J + 1$, if we assume the rigid rotator ap-

Table IV

^{12}CO Absorption at $V_{LSR} = -85.7$ km s^{-1}

Line	Observed ω (cm^{-1})	Velocity Shift (km s^{-1})	FWHM (km s^{-1})	Equivalent Width (cm^{-1})
R0	2147.816	−102.7	25.12	0.05010
P1	2140.179	−105.6	12.01	0.03221
R1	2151.607	−104.8	13.63	0.03561
P2	2136.302	−107.2	14.83	0.03725
R2	2155.329	−102.0	17.96	0.05420
P3	2132.369	−103.7	17.60	0.04265
R3	2159.074	−107.6	11.41	0.03379
P4	2128.445	−107.5	13.78	0.03702
R4	2162.768	−110.9	14.64	0.02746
P5	2124.449	−106.0	18.22	0.03646
R5	2166.358	−104.8	10.83	0.02446
P6	2120.423	−105.0	13.83	0.03267
R6	2169.936	−102.1	18.38	0.02769
P7	2116.371	−105.2	9.42	0.03323
P8	2112.269	−103.1	14.99	0.06858
R8	2177.086	−110.5	8.62	0.02314
P9	2108.193	−109.5	10.57	0.03166
R9	2180.531	−104.5	8.61	0.03791
P10	2104.047	−110.8	8.92	0.02440
P11	2099.863	−111.5	10.05	0.02025
P12	2095.596	−105.0	6.71	0.03334
P13	2091.465	−105.8	7.85	0.01853
P14	2087.074	−108.2	6.74	0.00903
P15	2082.745	−106.9	10.14	0.01803

proximation. Forming the ratio of the column densities in the J^{th} and zeroth rotational states yields $\frac{N_J}{N_0} = (2J+1)e^{-E_J/kT}$. Taking the logarithm of both sides yields the desired form: $\ln[N_J/2J+1] = \frac{E_J}{k}(-1/T)$ + constant. So, a plot of $\ln[N_J/2J+1]$ versus E_J/k should yield a straight line with slope = -1/T, under

Table V

^{13}CO Absorption at $V_{LSR} = -41.3$ km s^{-1}

Line	Observed ω (cm^{-1})	Rest ω (cm^{-1})	Velocity Shift (km s^{-1})	FWHM (km s^{-1})	Equivalent Width (cm^{-1})
R0	2100.140	2099.710	−61.5	10.61	0.03276
P1	2092.815	2092.391	−60.8	10.64	0.03149
P2	2089.116	2088.683	−62.3	11.23	0.04900
R2	2107.347	2106.898	−64.0	12.25	0.05243
P3	2085.374	2084.942	−62.2	14.06	0.05475
R3	2110.889	2110.442	−63.5	11.11	0.05008
P4	2081.603	2081.168	−62.6	11.27	0.04160
R5	2117.882	2117.431	−63.9	12.19	0.06228
R7	2124.743	2124.285	−64.7	12.70	0.03714
R9	2131.473	2131.005	−65.9	8.81	0.03219
R10	2134.771	2134.313	−64.4	14.84	0.03684
R11	2138.022	2137.588	−61.0	9.33	0.02118
R12	2141.288	2140.828	−64.5	10.96	0.03024
R13	2144.478	2144.034	−62.2	12.58	0.02791
R15	2150.764	2150.341	−59.0	10.36	0.02706
R16	2153.850	2153.442	−56.8	8.71	0.01170
R17	2156.933	2156.509	−59.0	9.26	0.01311
R18	2159.988	2159.540	−62.2	9.78	0.01441
R19	2162.957	2162.536	−58.4	9.76	0.01147
R21	2168.851	2168.422	−59.2	7.57	0.01308

the assumption of LTE.

Using the Boltzmann equation in an earlier form, it is possible to derive the total column density in a particular vibrational level. The partition function can be calculated for ^{12}CO and ^{13}CO provided the rotational constant, B_0, is known for each isotope of CO. The partition function for ^{12}CO and ^{13}CO is

Table VI

Summary of Velocities and Line Widths

Species	number of lines	V_{LSR} (km s^{-1})	FWHM (km s^{-1})	$\Delta v_{1/2}$ (km s^{-1})
^{12}CO	24	-43.9 ± 2.7	14.1 ± 3.2	11.6
^{12}CO	18	-54.4 ± 3.5	17.6 ± 10.9	15.7
^{12}CO	19	-72.6 ± 3.9	28.9 ± 14.7	27.8
^{12}CO	24	-85.7 ± 2.9	12.7 ± 4.5	9.9
^{13}CO	20	-41.3 ± 2.4	10.9 ± 1.8	7.4

$\mu(T) = 0.3616T + 1/3$ and $\mu(T) = 0.3782T + 1/3$, respectively. Using the temperatures estimated from the Boltzmann diagrams, we can calculate the total column density, N_T, in each rotational sublevel from the column density, N_J. The mean total column density can then be obtained by averaging over the individual determinations.

The relationship between the line strength and the column density is complicated if the lines are optically thick. A curve of growth analysis must be employed to estimate the column density in saturated lines. When the optical depth at the line center τ_0 is large, the equivalent width is related to the optical depth by $W_\omega = 2bF(\tau_0)/c$ where W_ω is the line strength in (cm^{-1}), b is a line width parameter, and $F(\tau_0)$ is a function dependent on the optical depth at line center and the velocity distribution of the absorbing gas. The parameter b in the above relation is given approximately by $b = \Delta v_{1/2}/2\sqrt{\ln 2}$ where $\Delta v_{1/2}$ is the intrinsic

line width. Spitzer (1978) tabulated the relationship between τ_0 and $F(\tau_0)$ assuming a Maxwellian velocity distribution. By solving for $F(\tau_0) = W_\omega c/2b$ with the known equivalent width and line width parameter, we can linearly interpolate in Table 3.1 (Spitzer 1978) to find τ_0. We can then compute the column density $N_J = \tau_0 b/1.497x10^{-2} f_J$ corrected for optical depth. As mentioned earlier, f_J is the transition probability of the J^{th} rotational state. With the corrected column density, the determination of the rotational temperature and the total column density proceed as outlined above.

Due to the saturated nature of the source velocity ^{12}CO lines, even the ^{13}CO may not be optically thin. So, a curve of growth analysis was employed to determine the column density in each rotational sublevel. The curve of growth, as described above, requires knowledge of the thermal line width parameter b. We computed b assuming $\Delta v_{1/2} = 7.4$ km s^{-1}. Table VII lists the line identification in column one, the column density computed assuming optically thin lines in column two, and the column density derived from a curve of growth analysis in column three. The corrected column densities are about a factor of 10 larger than the optically thin column density estimates. A large increase in the corrected column density usually indicates optically thick lines. The logarithm of the corrected column density is listed in column four; the rotational transition energy is listed in the last column. A Boltzmann diagram using the data in the last two columns in Table VII is shown in Figure 11.

Table VII

^{13}CO Column Densities at $V_{LSR} = -41.3$ km s^{-1}

Line	N_J (10^{16} cm^{-2})	Corrected N_J (10^{16} cm^{-2})	$\ln[N_J/2J+1]$	E/k (°K)
R0	0.38	4.42	38.33	0
P1	1.10	12.74	38.29	5.26
P2	1.43	18.18	38.13	15.77
R2	1.01	13.04	37.80	15.77
P3	1.50	19.67	37.87	31.54
R3	1.01	12.86	37.45	31.54
P4	1.10	13.41	37.24	52.56
R5	1.31	17.92	37.33	78.84
R7	7.96	9.65	36.40	147.16
R9	6.95	8.20	36.00	236.48
R10	0.80	9.65	36.06	289.02
R11	0.46	5.09	35.33	346.80
R12	0.66	7.65	35.66	409.82
R13	0.61	6.97	35.49	478.09
R15	0.59	6.72	35.31	630.33
R16	0.25	2.69	34.33	714.31
R17	0.28	3.03	34.39	803.51
R18	0.31	3.35	34.44	897.94
R19	0.29	2.62	34.14	997.60
R21	0.28	3.01	34.18	1212.57

The Boltzmann diagram indicates that two separate gas components are present along the line of sight to W3 IRS5. If the ^{13}CO lines were formed in LTE at a single temperature, then we would expect the data points to fall along a single straight line. As Figure 11 shows, a single straight line is a poor fit to the data. A better fit can be achieved if two straight lines are applied, one of shallow slope for $E/k \geq 100$°K and one of steep slope for $E/k \leq 100$°K. As Figure 12 shows,

the low J ($J \leq 5$) data points are well fit by a line corresponding to $T = 50^{+10}_{-7}$ K, and the high J ($J \geq 7$) points are represented by $T = 470^{+69}_{-53}$ K. The physical interpretation of these two temperatures will be discussed in Chapter Four.

The temperatures derived can be used to calculate the total column densities along the line of sight in the hot and warm cloud. Using the appropriate form of the Boltzmann equation with the ^{13}CO partition function given earlier, we find a total column density of 1.2×10^{17} cm^{-2} for the hot (470 K) gas and 1.1×10^{17} cm^{-2} for the warm (50 K) gas, for a total ^{13}CO column density of 2.3×10^{17} cm^{-2} along the line of sight to W3 IRS5.

The column density of ^{13}CO gas at the source velocity can be used to estimate the column density of ^{12}CO gas at the source velocity. By assuming an isotopic abundance ratio of ^{12}CO /^{13}CO = 60 (Wannier 1980), we calculate the ^{12}CO column density for the warm (50 K) gas to be 6.48×10^{18} cm^{-2}, and for the hot (470 K) gas, to be 7.08×10^{18} cm^{-2}. The column density of ^{12}CO gas at high velocities is small compared to the column density of source velocity ^{12}CO gas, so the total column density of ^{12}CO is 1.4×10^{19} cm^{-2}.

The ^{12}CO lin[illegible]t -54 km s^{-1} are heavily blended with the source velocity lines. Table VIII tabulates the derived column densities and transition energies for the absorption at -54 km s^{-1}. Column one lists the line identification, while column two lists the column density computed under the assumption of optical

thinness from the equivalent width presented in Table II . In column three, the logarithm of the column density is listed and in column four, the rotational transition energy is listed. A Boltzmann plot of the last two columns from Table VIII shows some curvature possibly present (see Figure 13). A linear least squares fit to the points yields T = 250^{+10}_{-7} K, which, when combined with the ^{12}CO partition function, yields an estimate for the total column density in this component of 1.6x10^{17} cm^{-2}. As Figure 13 shows, the data points have considerable scatter. The discussion is deferred until Chapter Four.

Since the -73 and -86 km s^{-1}components are part of the same broad feature, the data were combined in order to reduce the scatter. For rotational lines visible and measured in both velocity components, the equivalent widths were summed. The relative weakness of the absorption feature permits us to assume the lines are optically thin. Table IX presents the combined data for the high velocity feature. The line identifications are listed in column one. The equivalent width, for lines present in both Table III and IV are summed and listed in column two. The column density in column three is computed with the assumption that the lines are optically thin. The logarithm of the column density is listed in column four while the excitation energy of each transition is listed in column five.

A Boltzmann plot of the data in the last two columns in Table IX is given in Figure 14. A single temperature should result; however, there appears to be a

Table VIII

^{12}CO Column Densities at $V_{LSR} = -54.4$ km s^{-1}

Line	N_J (10^{16} cm^{-2})	$\ln[N_J/2J+1]$	E/k (°K)
R0	0.41	35.95	0
P2	0.53	34.60	16.50
R2	0.84	35.06	16.50
P4	1.20	34.86	54.98
R4	1.00	34.67	54.98
P5	0.59	33.92	82.47
R5	0.62	33.97	82.47
P6	1.20	34.43	115.45
R6	0.82	34.08	115.45
P7	0.88	34.01	153.93
R7	1.10	34.24	153.93
P8	1.20	34.17	197.90
R8	0.32	32.87	197.90
P9	0.92	33.81	247.36
R9	0.70	33.54	247.36
P12	1.30	33.85	428.67
P13	0.24	32.12	500.07
P15	0.55	32.81	659.31

break similar to that observed for ^{13}CO at about the same point in the diagram. We fit the data with two lines following the trend in the data, as shown in Figure 15. The points with $J \geq 6$ are best fit with line corresponding to $T = 400^{+65}_{-49}$ K, while the low $J \leq 5$ points correspond to $T = 60^{+13}_{-9}$ K. The total column density for the hot (400 K) gas is 2.5×10^{17} cm^{-2}, and for the warm (60 K) gas is 1.2×10^{17} cm^{-2}. A physical interpretation is given in Chapter Four.

Table IX

^{12}CO Column Densities, $V_{LSR} = -72.6$ & -85.7 km s^{-1}

Line	Equivalent Width (cm^{-2})	N_J (10^{16} cm^{-2})	$\ln[N_J/2J+1]$	E/k (°K)
P1	0.04964	1.664	36.25	5.50
R1	0.05585	0.929	35.67	5.50
P2	0.08175	2.289	36.06	16.50
P3	0.07821	2.049	35.61	32.99
R3	0.07515	1.452	35.27	32.99
P4	0.07784	1.971	35.32	54.98
R4	0.07118	1.411	34.99	54.98
P5	0.06628	1.645	34.94	82.47
R5	0.05291	1.066	34.51	82.47
P6	0.07321	1.794	34.86	115.45
R6	0.05590	1.138	34.41	115.45
P7	0.06939	1.686	34.66	153.93
P9	0.06902	1.661	34.40	247.36
P10	0.06128	1.470	34.18	302.31
P11	0.07514	1.800	34.29	362.74
P12	0.04672	1.118	33.73	428.67
P14	0.03773	0.902	33.37	576.95
P15	0.04827	1.154	33.55	659.31

Table X summarizes the temperature and column density results of our analysis. Columns one, two, and three identify the species, velocity, and rotational lines used in deriving the listed data. The rotational temperatures (with 1 σ errors) are listed in column four. Column five lists the total column density (with 1 σ errors) for the species listed in column one.

In Chapter Four we interpret these results comparing them to previous re-

Figure 11

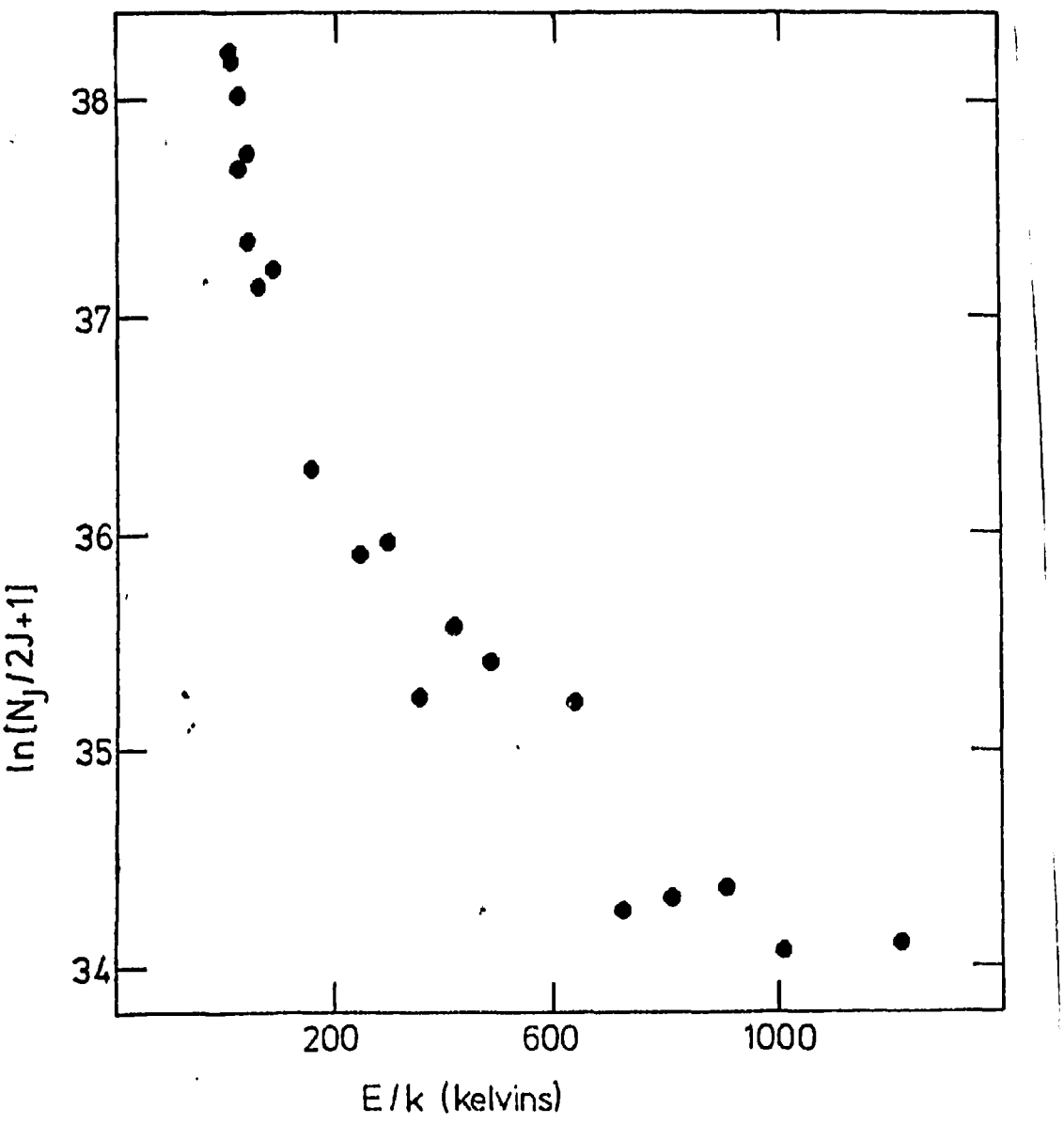

Boltzmann plot of ^{13}CO column densities corrected by a curve of growth analysis assuming b=7.4 km s^{-1}.

Figure 12

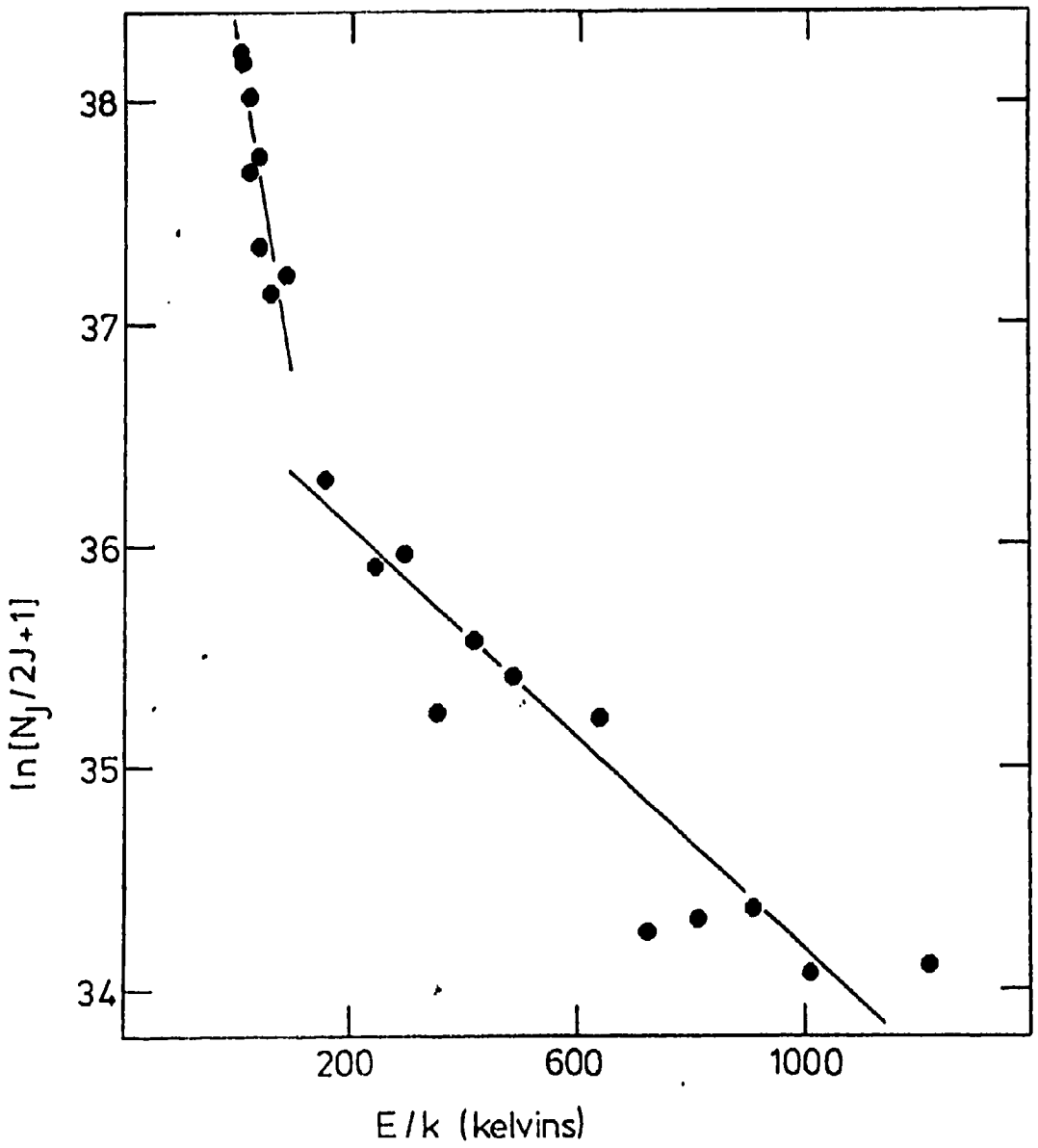

Same as Figure 11 with best fit lines drawn in for the low J and high J data points. The low J points are fit by a line of slope corresponding to T = 50°K, while high J points are fit by a line with slope corresponding to T = 470°K.

Figure 13

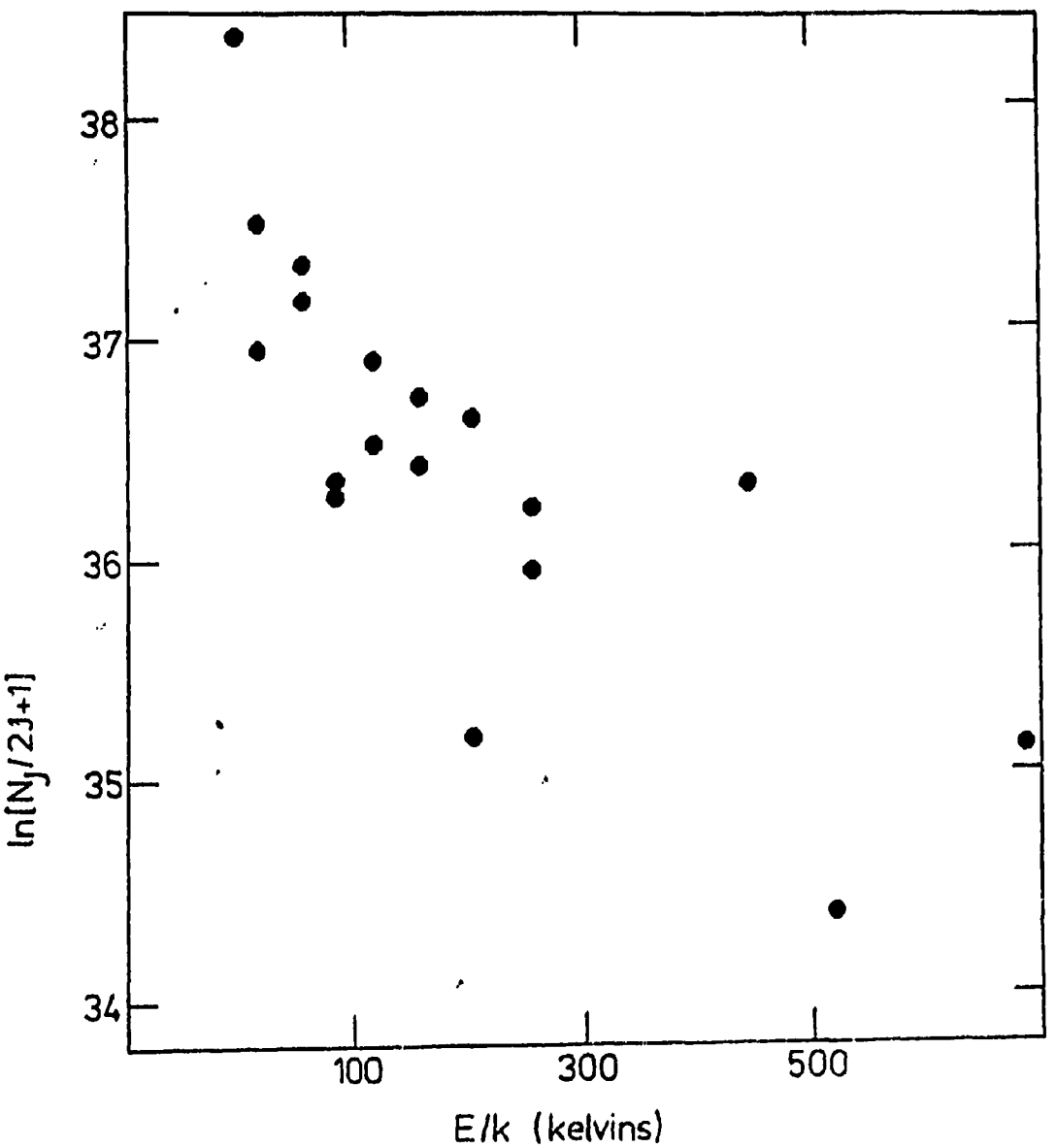

Boltzmann plot of ^{12}CO at -54 km s^{-1}. The column densities were computed directly under the assumption of optical thinness.

Figure 14

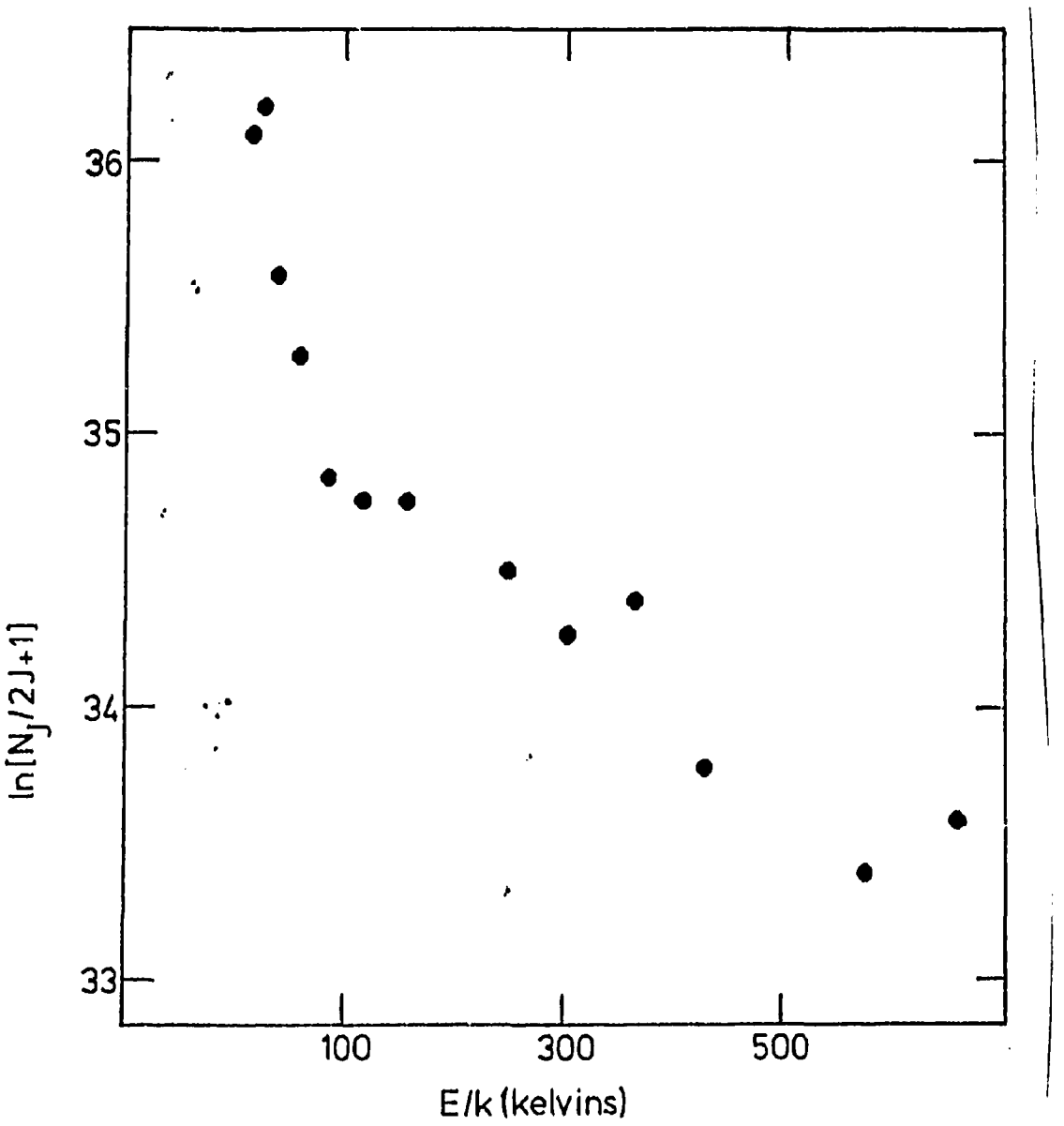

Boltzmann plot of ^{12}CO , combined high velocity data. The column densities were derived directly under the assumption of optical thinness.

Figure 15

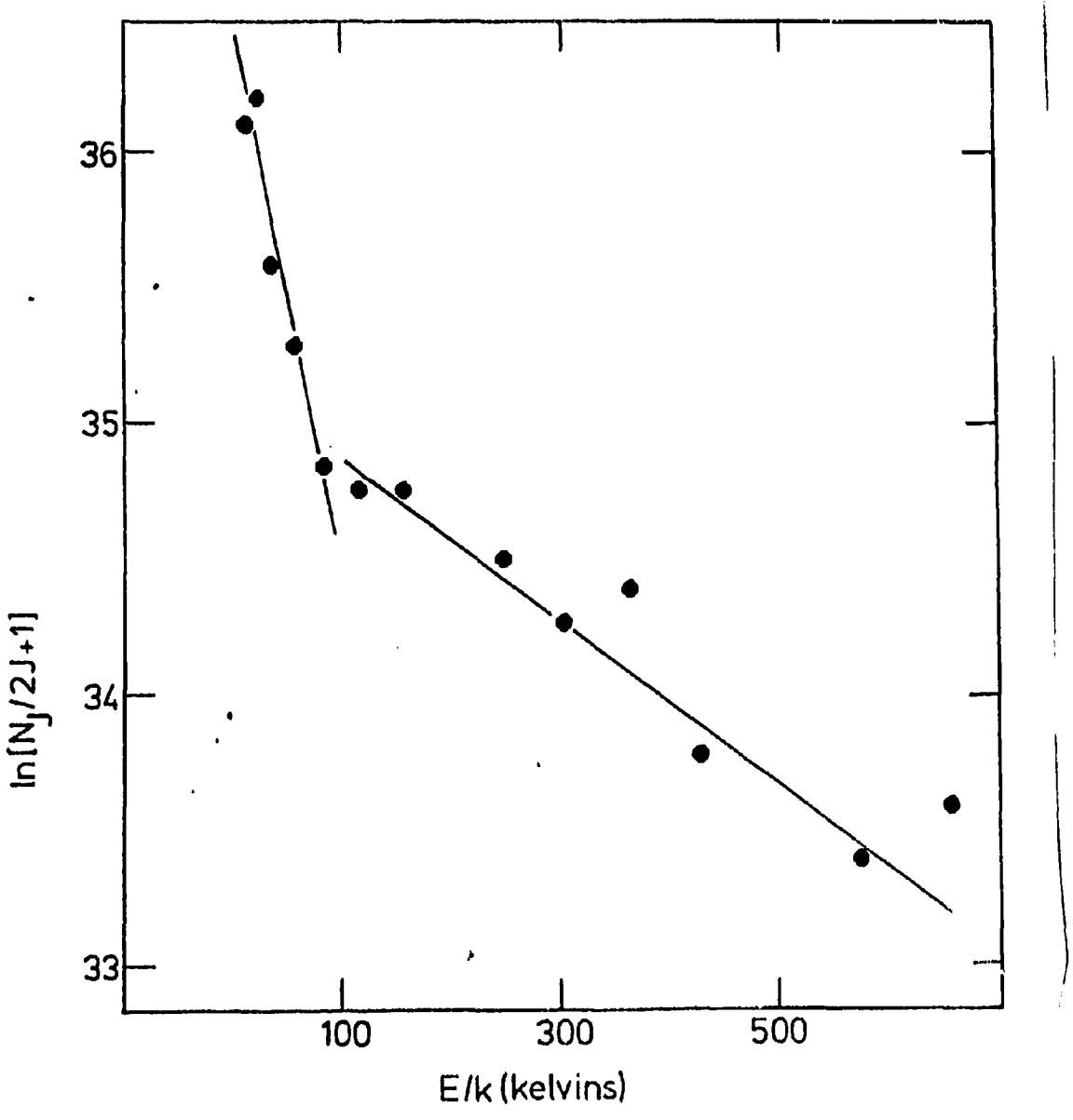

Same as Figure 14 with the best fit lines drawn in. The low J data are best fit with T = 60°K while the high J data are best represented by T = 400°K.

Table X

Summary of Temperatures and Column Densities

Species	V_{LSR} (km s^{-1})	J value	T (°K)	N_{Total} (10^{17} cm^{-2})
^{12}CO	-54.4	all J	250^{+10}_{-7}	1.59 ± 0.37
^{12}CO	high vel.	low J	60^{+13}_{-9}	1.17 ± 0.26
^{12}CO	high vel.	high J	400^{+65}_{-49}	2.50 ± 0.40
^{13}CO	-41.3	low J	50^{+10}_{-7}	1.08 ± 0.22
^{13}CO	-41.3	high J	470^{+69}_{-53}	1.18 ± 0.18

search on W3 IRS5 and we attempt to model this source in qualitative terms.

IV Discussion

The purpose of this project is to accurately determine the temperature, column density, and velocity structure of the molecular outflows associated with W3 IRS5. Comparison of our results with those of other massive young stars confirms the frequent occurrence of outflows while reinforcing the peculiar differences present in protostars of similar mass. Estimates of the outflow's dynamical ages can be used to indicate the frequency of occurrence during a star's pre-main-sequence lifetime. It is also important to investigate the depletion of CO onto grain mantles for possible effects on interstellar carbon chemistry. These are some of the important topics that need to be addressed.

Takano (1986) presented a simple relationship between the luminosity, of an embedded source, the dust temperature, T_d, and the distance of the dust from the source, given by

$$T_d = 70(2\text{x}10^{17}\text{cm/r})^{2/5}(L/10^5 L_\odot)^{1/5},$$

where r is the distance of the dust from the source in cm and L is the total luminosity of the source in solar units. Assuming the luminosity of W3 IRS5 is $6.9\text{x}10^5$ $L_\odot$ (Mozurkewich 1986), we can use the temperatures derived earlier to estimate the distance of the absorbing gas from the central source, provided that the dust and gas are well coupled.

Theory predicts that the dust and gas should be well coupled for densities $\geq 10^5$ cm^{-3} (Takano 1986). These densities are easily achieved close to the embedded source. Claussen *et al.* (1984) estimated the average density in the red and blue emission wings of ^{12}CO to be 10^5 cm^{-3}, which extend out to 8" (2.6×10^{17} cm) from W3 IRS5 and are adequate to provide good coupling between the dust and gas.

The data in the Boltzmann diagrams must be carefully interpreted. In LTE, the data points should fall along a straight line corresponding to a single temperature. The ^{13}CO Boltzmann diagram (Figure 12) clearly shows evidence for two straight lines. This implies two different temperature gas clouds along the line of sight are combining to produce this effect. Cloud superposition is reasonable and we assumed this in analysing the ^{13}CO lines.

If LTE does not apply, the determination of the gas temperature from the Boltzmann diagrams is more difficult. The data points in a Boltzmann diagram for a non-LTE gas cloud will not fall along a straight line. Instead, the data points should exhibit curvature which is different from that observed in our data. Since the curvature in our data is not representative of non-LTE gas conditi- ve analyse the data assuming LTE conditions exist.

As noted above, the best fit to the source velocity ^{13}CO Boltzmann plot (Figure 12) indicated that two discrete excitation temperatures were required to

adequately fit the data. The hot (470 K) gas is stationary with respect to W3 IRS5, and is probably near thermal equilibrium. An optically thick disk, rotationally supported and close to the source, should be rather uniform in temperature. The relationship of Takano (1986) with T_d = 470 K implies the hot ^{13}CO gas is about 300 AU distant. Therefore, a rotationally supported disk whose inner boundary is within 300 AU of a source of $6.9x10^5$ $L_\odot$ is capable of producing the hot (470 K) component of ^{13}CO gas observed.

This warm (50 K) gas is also stationary with respect to W3 IRS5. Using the expression of Takano (1986) with T_d = 50 K implies this warm stationary gas is about 0.4 parsecs from the source. This warm component can be associated with the ambient molecular cloud within which W3 IRS5 is embedded. This quiescent neutral gas can be seen to the west of W3 in Figure 1. Because this warm, neutral gas is stationary, it's temperature may be representative of the ambient molecular cloud as a whole.

Another possible interpretation of the data in the Boltzmann diagrams, besides two distinct temperatures, is that a temperature gradient may exist. Figure 13 is the Boltzmann diagram for the ^{12}CO -54 km s^{-1}gas. There is considerable scatter in the data, perhaps some curvature is present also. In this case, there do not appear to be two distinct temperature components as there are in Figure 12. Rather, a range of gas temperature between some minimum and maximum

is probably present in the gas. The most likely explanation of the -54 km s^{-1}gas is that the gas has acquired a temperature gradient since it was expelled. The straight line fit to the data yields a gas temperature between the maximum and minimum temperature possible for the data. Therefore, we fit the data in Figure 13 with a single straight line, corresponding to a temperature of 250 K, which is representative of the average gas temperature. Some of the scatter of the data in Figure 13 probably results from errors in the measuring process as well.

The -54 km s^{-1}data, can be used to yield an estimate of the flow's dynamical age. The expression of Takano (1986) with T_d = 250 K implies a distance of 1500 AU. Because this gas is receding from W3 IRS5 at about 13 km s^{-1}, we can estimate it's dynamical age. Under the assumption that the flow has expanded with constant velocity, its dynamical age is 530 years.

Although the data in Figure 14 seem to indicate two different temperature components are present, a small change in a couple of the data points may lead one to believe that some curvature is present instead. A temperature gradient is the preferred interpretation of Figure 14 as it is hard to understand how two distinct temperatures could arise in gas ejected from the source. We fit two temperatures to the data because it is useful to estimate both the column density and the range of temperatures present in the gas. The 60 K and 400 K gas probably represent the minimum and maximum gas temperature present in the cloud.

It is also possible to estimate the dynamical age of the high velocity flow. The expression of Takano (1986) with T_d = 400 K implies this component is 450 AU distant. We assume the expansion velocity of the gas to be the average of the two components (-73 and -86 km s^{-1}) less the source velocity (-41 km s^{-1}). The outflow velocity of 38.2 km s^{-1}, combined with its distance (assuming constant velocity) implies it is 60 years old. This is very important because W3 IRS5 has apparently undergone two or more outflow episodes in the last 500 years and because Mitchell *et al.* (1988b) detected a new outflow from M8E-IR which was also less than 100 years old.

The dynamical age of the outflows is extremely important because it can provide an estimate of the frequency of outflow occurrence. It would be useful to know if the outflows are truly sporadic, discrete events, as suggested by Mitchell *et al.* (1988d). The 250 K gas at -54 km s^{-1}has a dynamical age of 530 years while the 400 K gas at high velocities has a dynamical age of 60 years. Therefore, it appears that sporadic outflows occur at intervals of about 500 years or so. This is significant in that the frequency of molecular outflows is quite large if they continue at this rate over the star's pre–main–sequence lifetime. Because the kinetic energy in each flow is large and there are many flows, this process deposits large amounts of energy back into the molecular cloud. It is possible that this energy input into the clouds is largely responsible for the super- and hypersonic widths observed in molecular clouds. Obviously, outflows will be important in determining the

evolution of molecular clouds.

Lacy *et al.* (1984) obtained a low resolution 4.6 μm spectrum of W3 IRS5, and measured the equivalent width of solid ^{12}CO . They found $W_\omega = 0.9$ cm^{-1} which yields a ^{12}CO column density of $N_{solid} = 2x10^{17}$ cm^{-2}. The higher resolution spectrum presented in this thesis also shows absorption due to solid ^{12}CO (see Figure 10). The equivalent width of our solid ^{12}CO is $W_\omega = 1.0 \pm 0.1$ cm^{-1}, which agrees with $W_\omega = 0.9$ cm^{-1} found by Lacy *et al.* (1984).

Sandford *et al.* (1988) used experimentally determined data to obtain an accurate estimate of the solid absorption in W3 IRS5. They experimentally measured the absorption intensity parameter A, which is used in computing the total column density due to solid absorption. They determined A for pure solid CO rather than the value Lacy *et al.* (1984) used for CO in water ice. With this new value of the absorption intensity, Sandford *et al.* (1988) remeasured the spectra of Lacy *et al.* (1984) and obtained a value of $N_{solid} = 8.3x10^{16}$ cm^{-2} for the same feature. The value obtained by Sandford *et al.* (1988) is a more reliable estimate and we use it in computing the ratio of solid-to-gas ^{12}CO .

If we assume the solid CO grains to exist in the warm (50 K) ^{13}CO gas, we can estimate the solid-to-gas phase ratio in this quiescent neutral gas. Pure solid CO mantles exist only below 17 K (Leger 1983) so they cannot exist at 50 K temperatures. However, the addition of impurities into the CO mantles

raises the grain destruction temperature and allows the grains to exist at warmer temperatures (Leger 1983). Therefore, assuming some degree of imputities present in the CO mantles, we use the ^{13}CO column density for the warm (50 K) gas and ^{12}CO /^{13}CO = 60 (Wannier 1980) to compute the gas phase ^{12}CO column density. The solid ^{12}CO column density of Sandford *et al.* (1988) (8.3×10^{16} cm^{-2}) and the gas phase ^{12}CO column density (6.48×10^{18} cm^{-2}) yield the solid-to-gas phase ratio of 0.01.

If it is possible for CO to be locked into grains at much higher temperatures, then the total column density of ^{12}CO can be used to provide a lower limit to the solid-to-gas phase ratio. The gas phase ^{12}CO column density of 1.4×10^{19} cm^{-2} along with the solid ^{12}CO column density of Sandford *et al.* (1988) yields a solid-to-gas ratio of 0.006. Therefore, the local solid-to-gas ratio lies in the range 0.006–0.01, indicating that although some carbon has been removed from the gas phase, freezing out of carbon onto grains is not a significant factor affecting the gas phase chemistry of dense interstellar clouds near W3 IRS5. This result is entirely consistent with the solid-to-gas ratio determined for W33A by Mitchell *et al.* (1988c).

Bally and Lada (1983) obtained a ^{12}CO emission profile at 2.3 mm shown in Figure 16. Their emission exhibits wings of 52 km s^{-1}at the 100 mK level. Therefore, the outflow velocity is about 26 km s^{-1}. Our high resolution spectrum

shows line wings exceeding 65 km s^{-1}at the continuum, more than twice that reported by Bally and Lada (1983). Mitchell *et al.* (1988a, b) have shown that absorption spectroscopy is capable of detecting high velocity flows from YSOs that are not present in emission profiles.

An important question concerning molecular outflows, which has inspired some debate, is whether the outflows are expelled with their maximum velocity and decelerate as they expand away from the source or whether the outflows can be accelerated after leaving the source. First, only blueshifted absorption lines are observed in absorption spectra implying the gas is receding from the source towards the observer along the line of sight. Now, millimeter emission observations are capable of detecting high velocity, dense gas if it has a large enough beam filling factor. Because millimeter emission observations do not detect this high velocity gas, its filling factor must be small and hence the high velocity gas must be small in spatial extent. The most consistent and natural assumption is that the high velocity gas is still near the source that expelled it. This implies that the high velocity gas has just been ejected. Therefore, it is self-consistent to assume that the ejected gas is expelled with its highest velocity. As the ejected gas expands and increases in spatial extent, the beam filling factor for the gas increases as well. Eventually, the ejected gas may become detectable in millimeter emission surveys.

While this is a very simplistic interpretation, our results combined with a

Figure 16

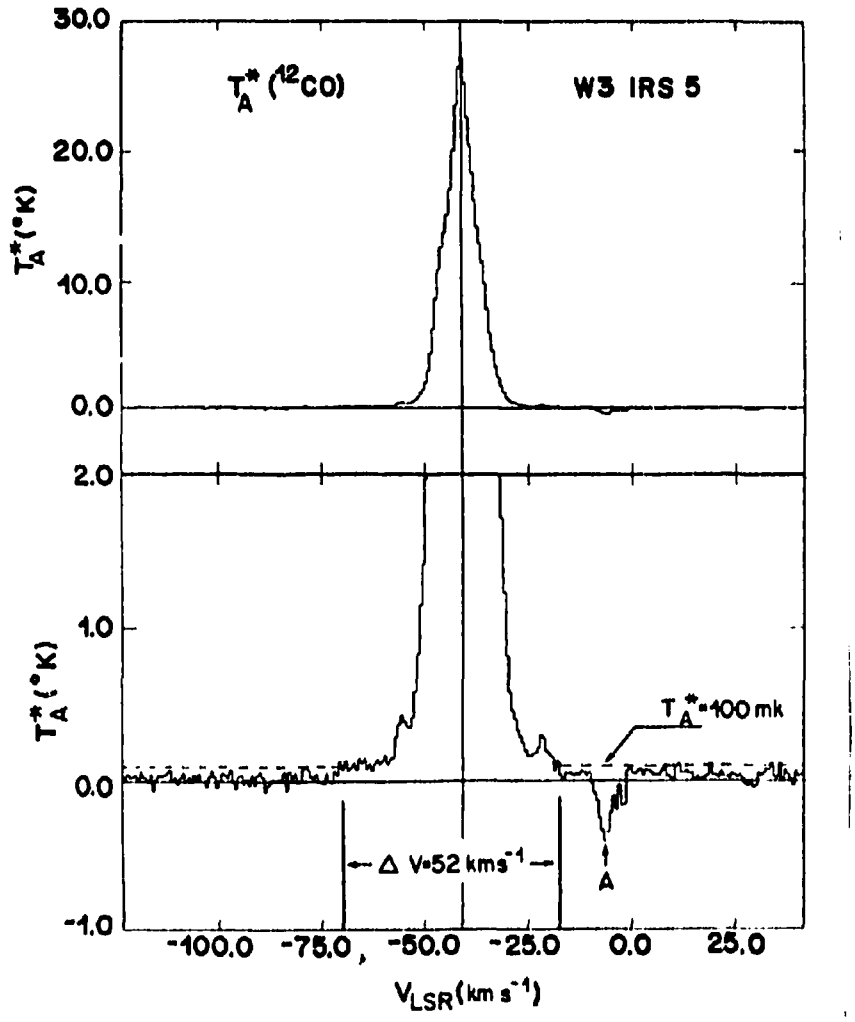

FIG. 5.—W3 IRS 5. The "absorption" feature marked A is a result of emission in the reference position.

W3 IRS5 (from Bally and Lada 1983). The "absorption" feature marked A is a result of emission in the reference position.

recent millimeter emission observation lend some credence to this idea. In our spectrum of W3 IRS5, three absorption lines are detected with velocities more negative than the source velocity (-54, -73, and -86 km s^{-1}), i.e., they are blueshifted. A recent millimeter emission observation shown in Figure 16 (from Bally and Lada 1983), shows no evidence, at the 100 mK level, of any emission at our highest detected velocities (-73 and -86 km s^{-1}). Their spectrum does, however, show a discrete peak at about -55 km s^{-1}which is where an absorption line is present in our spectrum. It is possible that the emission and absorption present at this velocity originates in the same gas. We previously estimated this absorbing gas to be at a distance of 1500 AU from the source and so it is fairly large in angular extent. The fact that the high velocity gas (-73 and -86 km s^{-1}) is not detected in emission is consistent with its being closer to the source than 1500 AU. If the above arguments are correct, a velocity gradient exists, supporting the idea that discrete outflows are expelled from the source with their maximum velocities and temperatures.

A schematic diagram of the various velocity components, their temperatures and distances from the central source is presented in Figure 17. The diagram is not drawn to scale.

It is important to demonstrate that our results are consistent with previous work on W3 IRS5. Our results are consistent with previous estimates of the

Figure 17

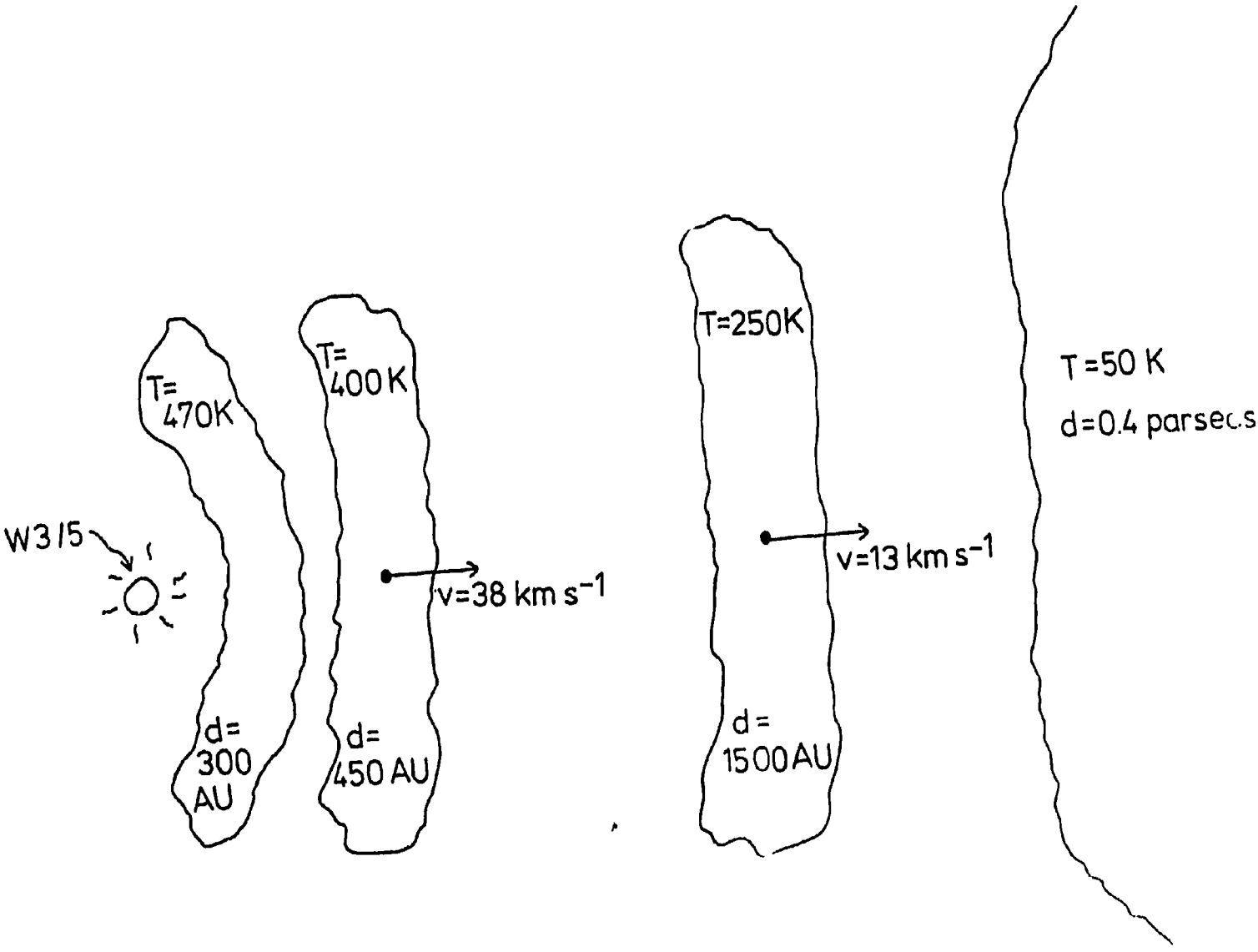

A schematic diagram showing the relative positions of sources of absorption near W3 IRS5. The positions, temperatures and velocities of specific features are indicated.

visual extinction in magnitudes, the ^{12}CO and ^{13}CO column densities, and the strength of the solid ^{12}CO absorption. It is interesting that the gas temperature surrounding W3 IRS5 is quite similar to the continuum (dust) temperature found in earlier studies.

First, we use the ^{13}CO column density to estimate the visual extinction in magnitudes. The total ^{13}CO column density, including the ^{12}CO components and assuming an isotopic abundance ratio of ^{12}CO /^{13}CO = 60 (Wannier 1980), is $\approx 2.2 \times 10^{17}$ cm^{-2}. If the standard relation between the total visual extinction and the total ^{13}CO column density is used, namely $N(^{13}CO) = 2 \times 10^{15}$ A_V, (Takano 1986), we find $A_V \approx 110$ magnitudes which is in reasonable agreement with the visual extinction implied by the large silicate optical depth of 7.64. Our result is also consistent with an upper limit of $A_V \leq 250$, deduced by Jaffe *et al.* (1984).

Thronson, Lada and Hewagama (1985) mapped the ^{13}CO emission over a small region centered about W3 IRS5 and determined the ^{13}CO column density was at least 1.2×10^{17} cm^{-2}. Our estimate is about a factor of two larger than their result. The results are consistent in that their emission map establishes only a lower limit to the ^{13}CO column density. It is not clear why our result is a factor of two larger, but beam dilution in their measurement may be an important consideration.

Estimates of the near-infrared continuum color temperature have ranged

from 350 to 900 K. Wynn-Williams, Becklin and Neugebauer (1972) and Willner *et al.* (1982) both estimated the continuum color temperature to be about 350 K using a 1–20 μm energy distribution (see Figure 18). Aitken and Jones (1973) determined the color temperature to be in the range 600–900 K with the large uncertainty due to circumstellar reddening. Our result of 470 K for the gas temperature is consistent with these previous estimates for the dust temperature. This result is important in that it is the first direct detection of the temperature of hot gas close to W3 IRS5 (within 300 AU).

W3 IRS5 has very strong silicate absorption at 9.7 μm (see Figure 18) which may originate in the same neutral gas as the solid CO. Lacy *et al.* (1984) used the optical depth of the 9.7 μm silicate absorption to estimate the ^{12}CO column density. The optical depth of the silicate absorption is $\tau_{9.7} = 7.64$. Using the relation $N(^{12}CO)/\tau_{9.7} = 1.3\text{x}10^{18}$ cm^{-2} they found $N(^{12}CO) = 1.0\text{x}10^{19}$ cm^{-2}, which is similar to the total ^{12}CO column density we derived of $N(^{12}CO) = 1.4\text{x}10^{19}$ cm^{-2}.

a. Summary

From a very high resolution spectrum of W3 IRS5 four ^{12}CO absorption components were detected. Mitchell *et al.* (1988d) postulated that such high velocity components result from sporadic outbursts of mass ejection. This conjecture is compatible with our results. The three high velocity ^{12}CO components (-54, -73 and -86 km s^{-1}) show a range in excitation temperature from 60 to 400 K with

Figure 18

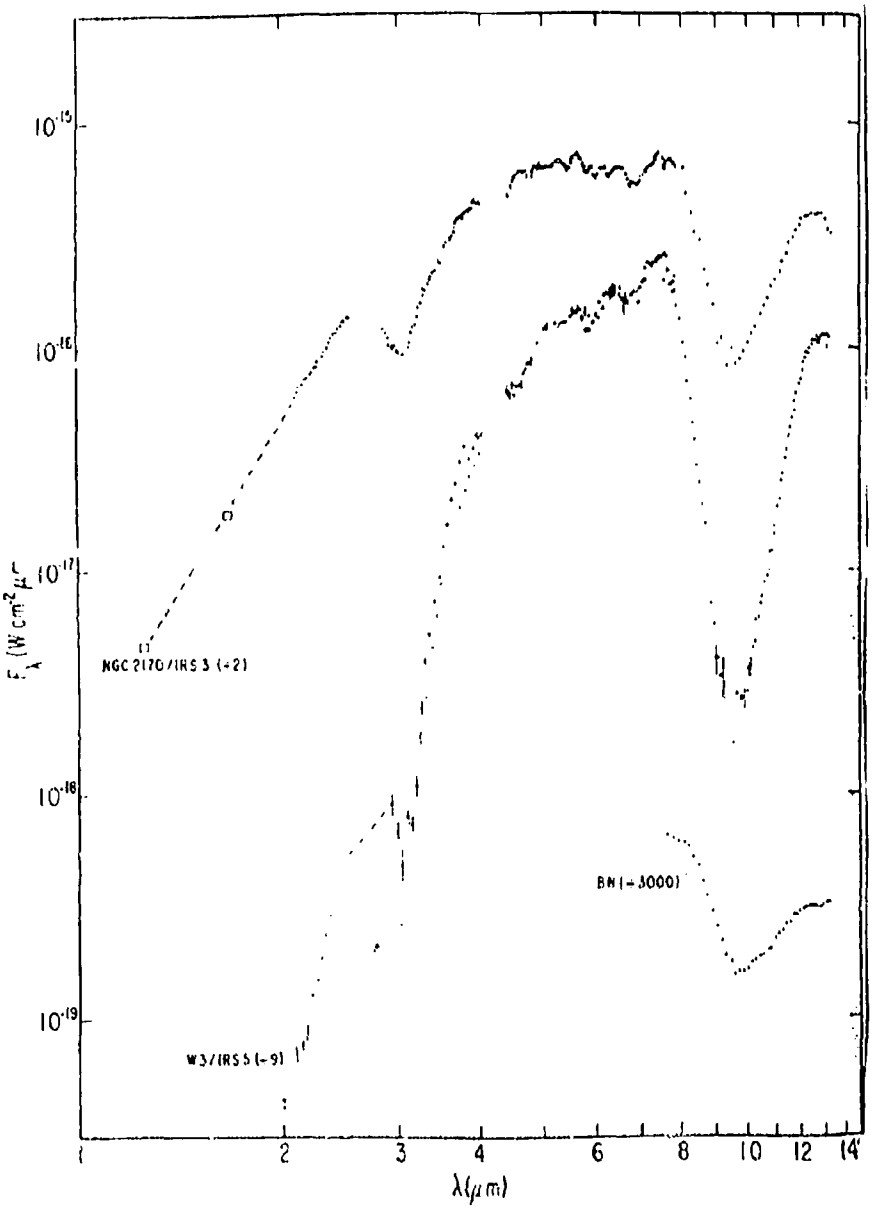

A 2-14 μm spectrum of W3 IRS5 (from Willner *et al.* 1982). Strong absorption at 9.7 μm is due to silicate ice and weaker absorption at 3.1 μm results from water ice.

temperature gradients possible within each velocity component. The question of whether high velocity flows are accelerated to their maximum velocity after they depart or whether they are ejected with their highest velocities is important. Our results suggest that the flows are ejected with their maximum velocity and are decelerated as they sweep up mass and move out from the driving source.

The ^{12}CO absorption features have a total velocity width in excess of 65 km s^{-1}, and so may be an important source of turbulent energy input into the cloud. The newly detected high velocity gas in W3 IRS5 is another example of the high level of flow activity present in many YSOs.

We measured ^{13}CO gas detectable at the source velocity and note the possible detection of a weak absorption component of ^{13}CO at -54 km s^{-1}. A spectrum with a higher S/N ratio would be capable of confirming this feature. The ambient cloud temperature as derived from ^{13}CO data is 50 K, which is consistent with cloud temperatures determined in regions where high mass star formation is taking place. We found the gas temperature near W3 IRS5 to be 470 K close (300 AU) to the source. It is interesting that previous estimates of the temperature due to infrared dust emission are similar to the gas temperature. This may indicate that the gas and dust are thermally coupled.

Our spectrum also shows absorption due to solid CO, and provides verification of the original detection by Lacy *et al.* (1984). The gas phase CO present

in our spectrum was used to derive a solid/gas phase ratio of 0.006–0.01, which is consistent with the solid/gas phase ratio of 0.01–0.03 found towards W33A by Mitchell *et al.* 1988c. This implies that the gas phase chemistry in dense interstellar clouds is not significantly affected by carbon depletion onto grain mantles.

Finally, the results of this thesis have demonstrated the importance of absorption spectroscopy in penetrating the highly obscured regions around protostars. Direct estimates of the column density and temperature are possible, and when combined with the velocity information, allow a more detailed understanding of the earliest stages of a star's life. Although several new and important results are presented, we do not yet have sufficient information to construct a coherent picture of the gaseous environment around W3 IRS5.

References

Aitken, D.K. and Jones, B. 1973, *Ap. J.*, **184**, 127.

Bally, J. and Lada, C.J. 1983, *Ap. J.*, **265**, 824.

Chandrasekhar, S. 1939, *An Introduction to Stellar Structure*. Chicago: University Chicago Press.

Claussen, M.J., Berge, G.L., Heiligman, G.M., Leighton, R.B., Lo, K.Y., Masson, C.R. Moffet, A.T., Phillips, T.G., Sargent, A.I., Scott, S.L., Wannier, P.G., and Woody, D.P. 1984, *Ap. J. Letters*, **285**, L79.

Dickel, H.R. 1980, *Ap. J.*, **238**, 829.

Dyck, H.M. and Howell, R.R. 1982, *Astron. J.*, **87**, 400.

Geballe, T.R. and Wade, R. 1985, *Ap. J. Letters*, **291**, L55.

Hall, D.N.B., Kleinmann, S.G., Ridgway, S.G., and Gillett, F.C. 1978, *Ap. J. Letters*, **223**, L47.

Heiles, C.H. 1987, In NATO/ASI *Physical Processes in Interstellar Clouds*, ed. M. Scholer, Dordrecht: Reidel.

Herbig, G.H. 1962, *Adv. Astron. Astrophys.*, **1**, 47.

Hollenbach, D.J., Werner, M.W., and Salpeter, E.E. 1971, *Ap. J.*, **163**, 165.

Jaffe, D.T., Hildebrand, R.H., Keene, J., and Whitcomb, S.E. 1984, *Ap. J. Letters*, **279**, L51.

Keto, E.R., Ho, P.T.P , and Haschick, A.D. 1987, *Ap. J.*, **318**, 712.

Kirby-Docken, K. and Liu, B. 1978, *Astrophys. J. Suppl. Series*, **36**, 359.

Lacy, J.H., Baas, F., Allamandola, L.J., Persson, S.E., McGregor, P.J., Lonsdale, C.J., Geballe, T.R., and Van De Bult, C.F.P. 1984, *Ap. J.*, **276**, 533.

Lada, C.J., Elmegreen, B.G., Cong, H., and Thaddeus, P. 1978, *Ap. J. Letters*, **226**, L39.

Lada, C.J. 1985, *Ann. Rev. Astron. Astrophys.*, **23**, 267.

Leger, A. 1983, *Astron. & Astrophys.*, **123**, 271.

Link, B. 1987, Fourier Transform Spectrometer Data Reduction Program User's Guide, CFHT Corporation.

Maillard, J.P., and Michel, G. 1982, in *IAU Colloquium 67, Instrumentation for Astronomy with Large Optical Telescopes*, ed. C.M. Humphries, Dordrecht: Reidel.

Mezger, P.G. and Smith, L.F. 1977 In *Star formation, IAU Symp. No. 75*, eds. T. de Jong and A. Maeder, Dordrecht: Reidel.

Mitchell, G.F., Curry, C., Maillard, J.P., and Allen, M. 1988a, *Ap. J.*, Submitted.

Mitchell, G.F., Allen, M., Beer, R., Dekany, R., Huntress, W., and Maillard, J.P. 1988b, *Ap. J. Letters*, **327**, L17.

Mitchell, G.F., Allen, M., and Maillard, J.P. 1988c, *Ap. J. Letters*, **333**, L55.

Mitchell, G.F., Allen, M., Beer, R., Dekany, R., Huntress, W., and Maillard, J.P. 1988d, *Astron. & Astrophys.*, **201**, L16.

Mozurkewich, D., Schwartz, P.R., and Smith, H.A. 1986, *Ap. J.*, **311**, 371.

Mundt, R. and Fried, J.W. 1983, *Ap. J. Letters*, **274**, L83.

Neugebauer, G., Becklin, E.E., and Matthews, K. 1982, *Astron. J.*, **87**, 395.

Parker, E.N. 1979, *Cosmical Magnetic Fields*, Oxford: Oxford University Press.

Pritchet, C. 1982, *Publ. Astron. Soc. Pacific*, **94**, 733.

Reid, M.J. and Moran, J.M. 198[illegible] *Ann. Rev. Astron. Astrophys.*, **19**, 231.

Sandford, S.A., Allamandola, L.J., Tielens, A.G.G.M., and Valero, G.J. 1988, *Ap. J.*, **329**, 498.

Schwartz, R.D. 1983, *Ann. Rev. Astron. Astrophys.*, **21**, 209.

Scoville, N.Z., Kleinmann, S.G., Hall, D.N.B., and Ridgway, S.T. 1983, *Ap. J.*, **275**, 201.

Shu, F.H. 1977, *Ap. J.*, **214**, 488.

Shu, F.H. 1985, In *The Milky Way, IAU Symp. No. 106*, eds. H. van Woerden, W.B. Burton and R.J. Allen, Dordrecht: Reidel.

Shu, F.H., Adams, F.C., and Lizano, S. 1987, *Ann. Rev. Astron. Astrophys.*, **25**, 23.

Simon, T., Simon, M., and Joyce, R.R. 1979, *Ap. J.*, **230**, 127.

Snell, R.L., Loren, R.B., and Plambeck, R.L. 1980, *Ap. J. Letters*, **239**, L17.

Solomon, P.M., Sanders, D.B., and Scoville, N.Z. 1979, In *The Large Scale Characteristics of Galaxies, IAU Symp. No. 84*, ed. W.B. Burton, Dordrecht: Reidel.

Solomon, P.M., Sanders, D.B., and Rivolo, A.R. 1985, *Ap. J. Letters*, **292**, L19.

Spitzer, L. Jr. 1978, *Physical Processes in the Interstellar Medium*, New York: Wiley-InterScience.

Strom, S.E., Strom, K.M., Grasdalen, G.L., Sellgren, K., and Wolff, S. 1985, *Astron. J.*, **90**, 2281.

Takano, T. 1986, *Ap. J.*, **303**, 349.

Thronson, H.A., Campbell, M.F., and Hoffmann, W.F. 1980, *Ap. J.*, **239**, 533.

Thronson, H.A., Lada, C.J., and Hewagama, T. 1985, *Ap. J.*, **297**, 662.

Wannier, P.G. 1980, *Ann. Rev. Astron. Astrophys.*, **18**, 399.

Welch, W.J., Vogel, S.N., Plambeck, R.L., Wright, M.C., and Bieging, J.H. 1985, *Science*, **228**, 1329.

Wells, D.C., Greisen, E.W., and Harten, R.H. 1981, *Astrophys. J. Suppl. Series*, **44**, 363.

Willner, S.P., Gillett, F.C., Herter, T.L., Jones, B., Krassner, J., Merrill, K.M., Pipher, J.L., Puetter, R.C., Rudy, R.J., Russell, R.W., and Soifer, B.T. 1982, *Ap. J.*, **253**, 174.

Wynn-Williams, C.G., Becklin, E.E., and Neugebauer, G. 1972, *M.N.R.A.S.*, **160**, 1.

Yuan, C. and Cassen, P. 1984, In *Protostars and Planets II*, eds. D.C. Black and M.S. Matthews, Tucson: University Arizona Press.

Zuckerman, B., and Palmer, P. 1974, *Ann. Rev. Astron. Astrophys.*, **12**, 279.

Appendix A

a. Program Description

The general trend in society today is toward an interactive familiarity with computers, and nowhere is this more visible than in modern science. A large fraction of current research in the physical sciences utilizes and requires large digital computers to acquire, manipulate and analyse scientific data. Astronomy is no exception to this, as anyone familar with current trends in astronomical research can attest.

The data for this thesis were acquired with a Fourier Transform Spectrometer, and were preprocessed by Dr. G.F. Mitchell at the Canada-France-Hawaii processing facility in Waimea, Hawaii, using FTS, the Fourier Transform Spectrometer Data Reduction Program, originally written by J.P. Maillard. The program FTS forms spectra from individual scans taken in Fourier space, by coadding and weighing the individual scans. The process of forming a spectrum from a number of individual scans increases the final spectrum S/N ratio. When a spectrum has been formed, the image is written on magnetic tape along with a header record which contains the final spectrum S/N ratio, integration time, airmass, UT time of observation, and other information. The header record directly precedes each spectrum on the tape. The tape containing the spectrum data files, and a program to read them, were

transported to Saint Marys University and downloaded onto the university VAX 11/780.

The primary stage of data reduction produces spectra from individual scans in Fourier space. The next stage of the reduction process is to locate interesting spectral features and measure accurately their positions, line strengths and widths. At the time this thesis was begun, a program known as Reticent, written by Chris Pritchet (1982), was available to manipulate digital spectrophotometric data. This program enables users to display, manipulate and measure spectra that are stored on magnetic tape in FITS format. This Flexible Image Transport System (FITS) method of storing digital data was developed to facilitate portability and encourage widespread use of a single format for astronomical data, see, for example, Wells *et al.* (1981). This is highly commendable; however, FTS data from the CFHT are not in FITS format, so Reticent could not be used directly. An attempt to translate the FTS data in their current format to a compatible FITS format for use with Reticent proved to be much more than a masters thesis project. Others e.g. Bob Link, (1987) have aready looked into ways to transform FTS data into FITS format. Also, it was suggested that we measure by hand, on a paper printout of the spectra, the positions, line strengths and other pertinent information. This process, while perfectly valid, is difficult in practice. I preferred to expend no small effort in developing a program that would allow

the user to display the spectra graphically on a terminal and measure them with reasonable accuracy.

b. General Use of Program

The program began as a simple routine to graphically display a portion of the spectrum on a Lanpar Vision II model 4214 terminal. The program allows the user flexibility in the graphics display, consistent data handling, and accurate line measurements. At this time, the basic program functions are: 1. to display spectra on a Tektronics compatible graphics terminal, 2. to allow the user control over the vertical/horizontal scale and shifting, 3. to allow the user to measure positions, line widths and line strengths, and 4. to generate a paper printout of any region of the spectrum.

c. Logging In

The user must have access to the account GRD:[GRD5036] on the VAX at Saint Marys. After logging on the VAX, you are at the system prompt. You must first locate the directory that contains the FTS data reduction program executable code and the data files; they will both be stored in the same directory. To do this type DA. You are now in the correct directory and may begin a reduction session. To bring up the program FTS, type RUN FTS. The program will prompt for the data files to use for this reduction

session and will then place the user in the main menu. From this menu, one can quit the program, by typing 'Q', and return to the system prompt.

While in the program the user is either in menu mode with the options listed or at a prompt for specific data. If in menu mode, a list of valid commands may be seen by typing 'H', for help. After the Help menu lists your options, it will return you to the same menu without a change of status. At any point in menu mode, the user may quit the program and return to the system by typing 'Q'. If the user is not in the main menu, type 'Q' several times until you are out of the program. Quitting in this fashion saves all relevant data and safely terminates program execution. Response to a prompt can be made in upper or lower case letters; there is no difference. Where numeric data are required, an example will be displayed or the user will be notified whether real or integer data are required. Real data must contain a decimal point. The program has been arranged as simply as possible to follow a "normal" sequence in the reduction of FTS data files. The author is open to suggestions on program improvement.

d. Adding New Spectra

The program uses the spectrum files created in the preprocessing stage with the file type *.spc. These spectrum files contain a header record (for a description of the header record, see Link 1987, Appendix A) and the spectral

data. The program requires all the spectra data files to reside in the same directory as the program executable module (GRD:[GRD5036.DATA]). When copying spectra (*.spc) files from the magnetic tape, place them into the directory GRD:[GRD5036.DATA]. The dot.spc data files must be renamed to be accessible to the program. The program reads all data files as FORTRAN device files, i.e. FOR0XX.DAT, where XX is a number between 10 and 99. By doing a directory listing at the system prompt, you can see a list of the current program data files. The new files must be renamed from *.spc to FOR0XX.DAT where XX is a number not currently assigned to another data file.

Next, the new data file must be entered in the file selection list. Determine if the new file is to be considered as a source or a standard, then edit the appropriate file source_names.for or stndrd_names.for. The format is self evident. Next, a small change to allow the user to select the new file number must be made. Again, edit the appropriate (source or standard) read_source.for or read_stndrd.for file and change the numeric range of valid file numbers to allow the file number to be read. This is all that must be done to include new data files to be processed with this program.

There are no files output by the program. The only file created by the program is the Zeta plot file which is deleted after it has been queued to the

Zeta plotter. When generating a Zeta plot file, all the user must do is walk to the computer room to gather the printout.

c. Program Logic and Calling Sequence

The program is menu driven for simplicity with all available options displayed in each menu. There are three separate menus used in the program. The main menu is the first and last menu the user sees when using the program. The option to produce a composite profile has its own menu. The options to display a ratio or to display two separate spectra share a single menu. These three menus share a common feature; the option 'H' always lists a brief description of all available options the user can select and the option 'Q' always quits the current menu and returns to the previously called menu. If the user is in the main menu, typing 'Q' exits the program and places the user back at the system prompt. The main menu has nine options, of which 'H' and 'Q' have the same meaning in each menu. They are 'B, C, D, I, H, Q, R, T, Z', which stand for Bin, Composite, Data, Information, Help, Quit, Ratio, Two, Zeta, respectively.

After the user has keyed 'RUN FTS' at the system prompt, the program initializes some program parameters and then immediately prompts the user to select a source and standard data file. The program lists each available data file by Fortran device number, from which the user must select one for

the source and one for the reference. Loading the database at the start of the program before the user reaches the main menu allows all the functions involving the spectra to draw from a single database. After the user has selected the two data files, the database is initialized and the main menu is displayed. The main menu options are described below.

The choice of 'D' in the main menu allows the user to reinitialize the database by selecting a new source and standard data file. The files are selected by the numbers displayed. The user must select a file, since no defaults are permitted. After successfully reinitializing the database, the main menu is again displayed.

The choice of 'I' in the main menu displays information extracted from the header record of the source and standard data file. When new data files are read, the information displayed in option 'I' is updated automatically. The information displayed includes the object name, date and time of observations, bandpass, observers comments, S/N ratio, airmass, and integration time.

The option to bin spectral data, option 'B', does not plot a spectrum on the terminal. Instead, the output is queued to and printed by the Zeta plotter. The choice of 'B' in the main menu allows the user to take any part of the spectrum, bin the data and plot them on the Zeta plotter. This can be useful

for displaying large (50 cm^{-1}) portions of the spectrum to show broad, weak features such as absorption by solid CO and "XCN" (tentatively identified as NCO^{+}). This option when selected prompts the user first for the left and right wavenumbers of the region to be displayed. Any numbers within the bandpass are acceptable; there are no limits on how many wavenumbers may be binned and plotted. Next, the user is prompted for the number of bins into which the intensity data should be placed, limited to 500 bins or less. Finally, the length of the x and y axis of the Zeta plot need to be specified. The axis length limits are $1 \leq x \leq 50$ and $1 \leq y \leq 10$, in inches. A final query is made allowing the user to return to the main menu without plotting the spectrum, if desired. When the output has been queued to the Zeta plotter, a message is typed on the terminal stating the job number and the plotter status. When the plot file has been spooled to the plotter, control is returned to the program and the main menu is redisplayed.

The option to plot a single spectrum, 'Z', does not display any data graphically on the terminal. The output is queued directly to the Zeta plotter. This routine also prompts for the left and right wavenumbers of the spectrum as well as the Zeta plot axis lengths, as in option 'B'. A choice is also available to quit prior to printing. The limits on the axis lengths and range of wavenumbers are the same as those in option 'B'. After the output is spooled to the Zeta plotter, control is returned to the main menu.

In the remaining three options, 'C', 'R' and 'T', spectra are always displayed on the graphics terminal. The letters stand for Composite, Ratio and Two, allowing the user to display on the terminal a kinematic line profile, the ratio of the source to standard star, or two individual spectra. Each of these options 'C', 'R' and 'T' has a submenu where the user is presented choices to change program parameters or measure the spectra. The options 'R' and 'T' share the same menu, since the user is likely to perform similar functions with these spectra. The submenu in the composite option does not allow the user to measure the composite profile, so a different menu is displayed. A flow chart showing the calling sequence of the main menu and the two secondary menus is given in Appendix B. A description of these three options and the submenus is given below.

The last three options of the main menu, 'C', 'R' and 'T', all graphically display spectra on the terminal. The two submenus in each of these options share common features that are desirable whenever spectra are plotted on the terminal. The common options in the submenus are 'C, H, L, P, Q, V, W, Z', which stand for Cut, Help, List, Paste, Quit, Vertical scale, Wavenumber scale, Zeta plot. The options 'H' and 'Q' have their usual meaning. The choice to cut/paste allows the user to remove/replace a portion of the spectrum from the graphic display. This is particularly useful for removing spikes in ratioed spectra. The user may replace a cut region by using the paste op-

tion. The option 'L' displays a list of the regions (left and right margins) cut from the spectrum in pixels. To replace or paste a cut portion of the displayed spectrum, the user must enter the left edge of the cut region in pixels, which is displayed in option 'L'. The graphic display may be altered by using the options 'V' and 'W', which change the vertical and horizontal scaling of the data displayed. Option 'V' allows a range from [1...9] inclusive; with V=1 the data are vertically stretched to cover the entire screen, while with V=9 the data are compressed vertically so that they cover only $1/9^{th}$ the screen. Option 'W' changes the wavenumber range displayed, with the allowed range [from 1...200 wavenumbers] to be displayed. The screen has only 1024 horizontal addressable pixels, so that if more than 20 wavenumbers are selected, the data are automatically binned and displayed as such. If the range of wavenumbers is ≤ 20, the data are displayed normally. The final common option of 'C', 'R' and 'T' is option 'Z', which generates a Zeta plot file of the spectrum currently displayed on the screen. The user must again specify the x and y axis lengths of the Zeta printout, after which the plot file is automatically queued to the Zeta plotter. The previously displayed spectrum is replotted and the appropriate menu redisplayed.

Besides these eight shared features, there are two options that are unique to the composite menu, and five options that are unique to the menu shared by 'R' and 'T'. The two additional options in the composite are 'A' and 'D'

which allow the user to add a new line or to delete a line from the composite profile. The five additional options in 'R' and 'T' are 'E, F, N, X, Y', which stand for Equivalent width, Full width, New wavenumber, X shift and Y shift. Option 'E' allows the user to measure the equivalent width of emission and absorption lines. Option 'F' measures the line center and FWHM of spectral lines. Option 'N' allows the user to change the wavenumber of the spectral region displayed. Option 'X' allows the user to horizontally shift the source spectrum relative to the standard star. Option 'Y' allows the user to vertically shift the source spectrum relative to the standard.

Option 'C' in the main menu will bring up the subprogram to produce a composite line profile. The program allows the user to form a composite line profile from the sum of up to 30 different lines. The composite line profile will coadd a maximum of 30 separate lines in velocity space and then display the composite profile on the graphics terminal. Each line position should have its vertical and horizontal shift entered so that each individual line will represent a best fit to the continuum. The line positions entered are assumed to be at a velocity of zero km s^{-1}. Each line requires a different vertical and horizontal shift in order to provide a best fit to the continuum. When the line positions are entered, the shifts should be entered so the ratioed result is best for each line. The width of the display in velocity space depends on the wavenumber range the user has selected. The default wavenumber range is initially

2 cm^{-1} or 300 km s^{-1} in the wavenumber range used here. If the user selects a larger range for display, the profiles are converted from wavenumber space to the new velocity space and coadded accordingly. Each line profile is computed over the same velocity range which, initially, is $\sim$ 150 km s^{-1} to the red and blue of the line positions entered. After each of the lines has been computed in velocity space, they are shifted, ratioed, coadded and displayed as a composite profile. The program requires many cpu seconds to compute the results and display them on the terminal. If 20 lines are being coadded, it is not unreasonable to require 20 cpu seconds (i.e. approximately 1 cpu second for each line coadded). Thus, while it may seem that the program is idle, stand by; it is working hard.

When the composite profile is displayed on the terminal, it is automatically vertically centered in the screen. Sometimes the composite line profile will be displayed as a nearly straight line from edge to edge. This is because strong telluric absorption has created a "spike" in the ratio, so that, when the program scales the data, the spectrum is flattened to accommodate the spike on the screen. It is a simple matter to cut the spike from the display to allow the spectrum to be viewed at a reasonable scale. There may be multiple spikes in some profiles, requiring the user to cut the spikes out individually.

After the desired number of lines have been coadded and the spikes have

been removed, the user may wish to plot this composite profile on the Zeta plotter. To do this, option 'Z' should be entered. This choice will prompt for the x and y axis lengths for the Zeta printout. After the Zeta plot file has been assembled, it will query the user to confirm that this file is to be printed. If not, the spectrum is replotted and the user is returned to the composite menu.

The program also allows the user to plot the source and standard spectra separately on the screen. The program will prompt for the wavenumber of the desired spectral region, and plot both spectra on the terminal. Note that vertical shifting always shifts the source spectrum relative to the standard spectrum. After the spectra are plotted, a list of options is presented where 'Q' and 'H' have their normal meaning.

The program also allows the user to plot the ratioed spectrum of the source to standard star. The user should enter 'R' in the main menu to plot a ratio. The central wavenumber must be entered, the two spectra are ratioed point by point, and plotted on the screen. The ratio will occasionally produce spikes. Because the program automatically vertically scales the screen display, these spikes may reduce the size of the feature the user wants to see. To alleviate the problem of these spikes distorting the intensity scale, the user is given the option of cutting them out of the visual display using

option 'C'. The program will then replot the data with the spikes removed, and will enlarge the vertical (intensity) scale. Also plotted in the ratioed spectrum is a horizontal line which represents a ratio value of unity. This line can be considered to be the continuum (where the source intensity equals the reference intensity) and is useful when trying to match the continuum of the source and standard since it forms a reference feature to which the ratio continuum can be matched. At this point, it would be reasonable to measure the equivalent width of the source lines.

Appendix B

a. Flow Charts

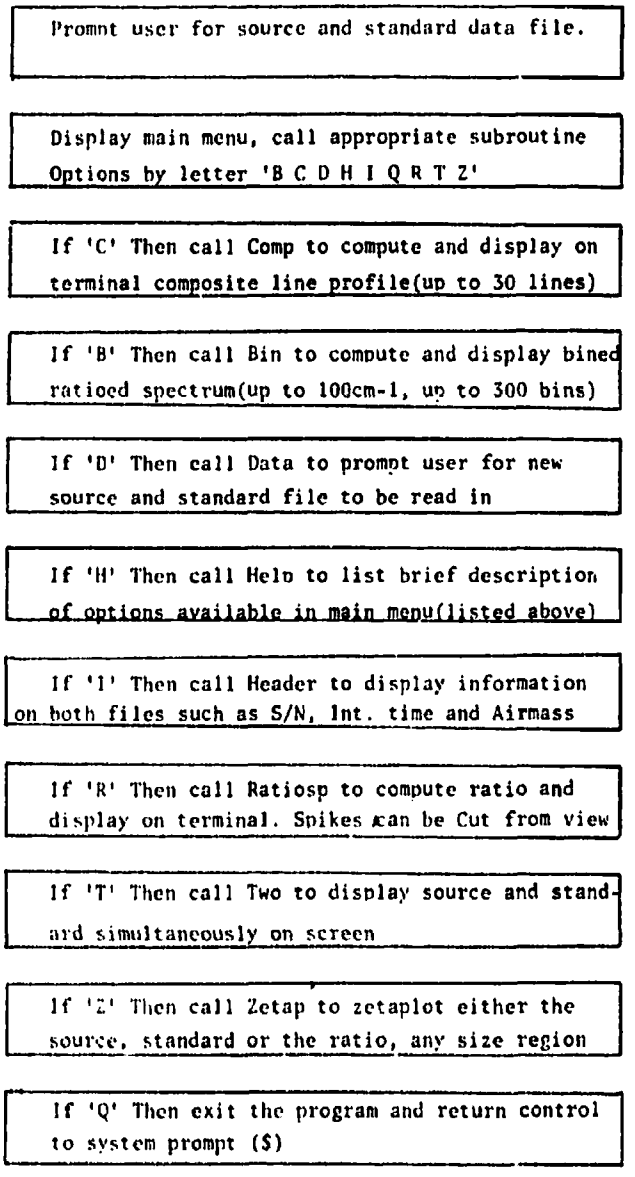

Appendix C

a. Subroutine Descriptions

A detailed description of all program routines is given below. The routines have been broadly grouped by function. The groups are a.) Main program modules which are the subroutines called directly from the main menu, b.) File handling routines, c.) Graphic display routines which are involved in setting the terminal for plotting, d.) Computational routines which interpolate, iterate or compute for general purpose, e.) The rest of the flock.

b. Main Program Modules

RPFTS – This is the main program segment. It is the only entry and exit point for the program. The main menu consists of nine options 'B, C, D, H, I, Q, R, T, Z', which are only called from and always return to the main menu.

Bin – This module is called from the main menu when 'B' has been entered. It displays binned data on the terminal for any spectral region inside the bandpass (up to 100 wavenumbers). The user may supply the number of bins or it defaults to the wavenumber range.

Comp – The subroutine to produce a composite line profile is called when a 'C' is entered in the main menu. This subprogram is used to coadd up to 30 lines in

velocity space and display the resulting line profile on the terminal. It requires the user to enter the line center of the line to be coadded, the horizontal and vertical shift (if non-zero). It forms the ratio of the source to the standard for each line and then coadds each line coherently in velocity space.

Data – This module is called to read in a new database, when the user enters option 'D' in the main menu. This routine calls Read_source, Read_stndrd, to display available data files and prompt the user for the new data files to be read in.

Helpmain – The general help facility is always involked by typing 'H' at any menu prompt throughout the program. This routine types out brief descriptions of the nine available options in the main menu. It returns the user to the main menu when finished.

Information – This module is called by the main menu when the user enters option 'I'. It displays information extracted from the header records from the source and standard data files that the user may find useful. It lists the object name, date of observation, bandpass, observer's comments, integration time, signal/noise ratio and airmass for both data files.

Ratiosp – This is involked by typing 'R' in the main menu. It is used to ratio a source and standard file and display the output on the graphics terminal. It

requires as input the line position on which to center the spectrum as well as the wavenumber range to display. Any line position inside the bandpass is valid and from 1...100 wavenumbers may be displayed on the terminal. If more than about 23 wavenumbers are to be plotted the data are binned to increase the resolution of the display.

Two – This routine is called when 'T' is entered in the main menu. It plots the source and standard spectrum together on the screen. It requests the wavenumber and range of the terminal display. The two spectra may be shifted vertically (to match the continua) or horizontally.

Zetap – This routine is called when 'Z' is entered in the main menu. It plots on the Zeta plotter either the source or standard spectrum, not ratioed. It prompts the user to select the source or standard file, the wavenumber range for plotting and the x and y axis length. It returns the user to the main menu when the output has been queued to the zeta plotter.

c. File Handling Routines

Read_Source – This subroutine prompts the user for the new source file and then reads it into the database. If new source data files are to be added to the program, this module must be updated.

Read_Stndrd – This subroutine prompts the user for the new standard file and reads it into the database. A check is made to ensure the user has selected the same bandpass for both the source and standard data files. If different bandpasses have been selected, the program requires the user to select another standard data file compatible with the selected source data file. If new standard data files are to be added to the program, this module must be updated.

Source_Names – This module lists all source data files available to the program, by Fortran device number. If new source data files are to be added to the program, this module must be updated.

Stndrd_Names – This module lists all standard data files available to the program and must also be updated if new standard data files are added.

d. Graphic Display Routines

Clr_Scn – This module sends an escape sequence to the Lanpar terminal to clear the graphics screen.

Cup – This routine positions the graphic cursor to the correct pixel location and turns on the pixel at that location.

Gmode – This routine sends an escape sequence to the Lanpar terminal which sets the screen to graphics mode.

Plot_Screen – This routine takes the interpolated, scaled spectral data and plots them on the graphics screen. It plots 1024 (nxpixels) pixels each time it plots a spectrum. If two spectra are plotted, it plots 2*1024.

Tmode – This routine sends an escape sequence to the Lanpar terminal which sets the screen to terminal (ANSI) mode.

X_Hair – This module sends an escape sequence to the Lanpar telling it to make the crosshairs visible. The position of the vertical thread is used for communicating the user's choice of line positions in the spectrum to the program. The user should position the crosshairs using the four arrow keys to the right of the "return" key. The crosshairs move at two speeds; high speed is achieved when the arrow key has been held down for more than two seconds. The crosshairs move one pixel each time the arrow key is pressed and released. Sometimes the crosshairs do not move on the screen when the arrow key is pressed. There is nothing wrong. The graphics plane is slightly curved so that every fifth or sixth pixel corresponds to the same crosshair position. There are 1024 by 823 pixels in the graphics plane.

Xhairposn – This routine is called following X_Hair to determine the position of the cross hair. The x and y pixel coordinates are put into a common variable for other routines which require them.

e. Computational Routines

Addlne - This module is called only by Composite, and is used to enter lines to be added to the composite profile. The routine prompts for the line center (in cm^{-1}), the vertical shift (intensity units) and the horizontal shift (in 0.02 cm^{-1}). The user may just type "return" for the horizontal and vertical shift; the program assumes a value of zero. To stop adding new lines, the user should type a "return" at the prompt for "new line to add". The program will then plot out the new composite profile and return the user to the composite menu.

Bindata – This routines prompts user for the number of bins, otherwise it defaults setting nbins=wvnr. It then interpolates the spectrum over the desired region and bins the data for display.

Cut – This module calls X_Hair to put the cross hairs on the screen, and allows the user to cut out undesirable regions of the displayed spectrum. If the cross hairs are not moved, no region is cut. If portions of the currently cut regions overlap the new region cut, a larger single cut region is formed from the two or more overlapping regions.

Dellne – This module is called only by Composite and it allows the user to delete a line from the composite profile. The routine prompts for the line center to be deleted. If it is not found, a message will state this and will reprompt the user for the line. The line center and line shift data will be deleted from the composite line list. This routine only allows one line to be deleted at a time. After a line

has been deleted, the new composite spectrum is plotted and the composite menu displayed. If the user does not wish to delete a line, he may just type a return at the prompt and no lines will be deleted; the same spectrum will be plotted and the composite menu displayed.

Eqvwth – This module is called from option and measures the equivalent widths of absorption and emission lines in the spectrum. It also gives a value for the full width at zero intensity (FWZI) of the line being measured. The program puts a set of crosshairs on the screen; the user should position the vertical thread to first one edge, then the other side of the line they want to measure. The vertical thread must be placed exactly at the edge where the user thinks the line profile joins the continuum. The program then integrates over the emission/absorption line to find the equivalent width . It computes the FWZI by taking the left and right line edges, converts them to wavenumbers and uses the standard Doppler relation to compute the velocity width. The line center is assumed to lie halfway between the left and right margins. The FWZI is displayed in km s^{-1}, the equivalent width in cm^{-1}.

Flwh – This module is called from options and it determines the line position and measures the FWHM for both absorption and emission lines. A set of crosshairs placed on the screen may be moved using the four arrow keys. The vertical thread must be placed at the position of the line center. The horizontal thread positioning

is not critical as it is not used. The program reads the pixel position of the vertical thread and converts it to an equivalent wavenumber, the position of the line center. The program uses the position of the line center to compute the half intensity and hence the FWHM. The FWHM is computed differently depending on whether the displayed spectrum is a ratio, 'R', or two separate spectra, 'T'. If the ratio is displayed, the FWHM is computed by taking the ratioed intensity at the line center (for absorption lines, this would be ≤ 1) and computing the half-intensity point relative to the continuum (straight line displayed on the screen). Then, the ratioed intensity of the line profile is checked, until it is greater than the half-intensity. This is done on both the red and blue sides of the line center until the half-intensity is reached or a maximum FWHM $\sim$ 150 km s^{-1} has been exceeded. If two spectra are displayed, the FWHM is computed by taking the source intensity at the line center and the standard intensity at the line center and determining the half-intensity value for the ratioed spectrum. The source profile is followed until the source intensity is less than the half intensity. The profile is again followed to both the red and blue of the line center. The FWHM in both the ratio and two spectra display is computed using the full width of the line in wavenumbers and the line center as marked by the vertical crosshair. The line center is displayed in cm^{-1}, the FWHM is given in km s^{-1}. The program also estimates the FWHM by taking twice the narrower of the two half widths. This value (NFWHM) is always less than the FWHM and in some cases is a much better estimate of the true FWHM. For lines which are strongly blended on one side, the FWHM may

be very large ($\sim$ 50 km s^{-1}) while the NFWHM may be quite reasonable. It is up to the user to decide which line width estimate to use.

Interpolate – This routine is called by Composite and option. It is called whenever the total number of data points for display is less than the number of pixels available, i.e. whenever the wavenumber range is less than or equal to 20 cm^{-1}. It performs a cubic spline fit to the data and returns an array with 1024 data points interpolated in intensity and wavenumber. This routine calls Spl3, Zspl3 and Tri, which are used in fitting a cubic spline to the data.

Lncntr – This module is called when the user is adding or removing lines from the composite spectrum. It verifies the line entered is valid and enters it into the lnctr array of line centers.

Paste – This routine is called by option and Composite. It replaces a region cut from the display. It requires the user to enter the left edge of the cut region, as given by option 'L'. The spectrum is replotted with the cut region replaced and the appropriate menu is displayed.

Plotzetafil – This is called by all routines generating a zeta plot file. It prompts the user to return to the called menu without plotting; otherwise it issues a system request to spawn a subprocess which will queue the zeta plot file to the zeta printer.

Prep – It takes the wavenumber, the range of wavenumbers and the vertical and horizontal shifts and extracts the necessary data from the database. After the data have been prepped, interpolate is called to provide a smooth fit to the raw data. On completion of this routine, an array of 1024 data points, consisting of interpolated intensities and wavenumbers, is ready to be plotted.

Ratio_Trn – This routine is called by ratiosp and performs the same functions as trans except that it operates on a single ratioed spectrum instead of two spectra. The data used as input to this routine are prepared in the subroutine ratiosp.

Spl3 – This routine is called by Interpolate to build a 3D matrix for fitting the cubic spline.

Trans – This routine is called by Two directly after prep has been called. This routine takes the shifted, interpolated data and transforms the real units (intensity and wavenumbers) to pixel units for display on the terminal. The pixel data are then vertically scaled to the users selection (option 'V'), and if any regions have been cut, the pixel values are set to zero in these cut regions. Any pixel values of zero are not plotted by the program.

Tri – This routine is called by Interpolate and it tri-diagonalizes the matrix to find the roots of the cubic spline.

Zetabin – This module is called by Bin and is used to create a zeta plot file of the binned spectrum currently displayed on the terminal.

Zetacomp – This module is called by Comp and is used to create a zeta plot file of the composite line profile currently displayed on the terminal.

Zetapf – This routine is shared by Two and Ratiosp. It produces a zeta plot file of the currently displayed spectrum on the terminal. If two spectra are displayed, both appear in the zeta printout. If spectral regions have been Cut, they will also be missing from the printout.

Zspl3 – This routine is called by interpolate and is used to fill the output array with the interpolated values.

f. Parameter Routines

Helpcomp – This routine types out brief descriptions for the 10 options available in the composite menu.

Helptandr – This routine types out brief descriptions for the 14 options available to the user in the option menu.

Hshift – This routine is called from option; it displays the current horizontal shift and reads the new horizontal shift desired. The shift read in is added to that

already selected. The shift is applied to the source data so the source spectrum is shifted relative to the standard spectrum. This shift is based on the number of sample points per wavenumber in the original spectrum. The shift is in sample points. There are approximately 43 sample points per wavenumber so a shift of 43 will offset the source data by one wavenumber from the positions of the reference data.

Init – This routine initializes an array used in transforming the spectral data to pixel data for display on the terminal. It also defines the number of x and y pixels available for plotting and a number of flags used in the program.

Optionbin – This module displays the menu of all available options for the user in Bin. It parses the user's selection and calls the appropriate subroutine to process the request.

Optioncomp – This routine displays the menu of all available options for the user in Comp. It parses the request and calls the proper subroutine.

Optiontandr – This routine displays the menu of available options in the subroutines Two and Ratiosp. The options are the same for both routines, as the processing is nearly identical. It parses the user's request and calls the appropriate subroutine.

Read_Wvn – This routine is called by option. It displays the current wavenumber and prompts for the new value. It checks to see that the value is inside the bandpass. If no value is entered, the current value is used. The first time through the program, the default value is computed as the exact midpoint of the bandpass (approximately 2119 cm^{-1}).

Read_Wvnr – This routine is called by options to select a different range of wavenumbers for graphic display. Each time a new wavenumber is selected, the range is set to two wavenumbers. The program allows the user to display from one to 100 wavenumbers on the screen at once. If more than about 23 wavenumbers are requested, the spectral region is binned.

Sholne – This module is called by Composite to display a list of the line positions, vertical and horizontal shifts of all the lines currently being used in the composite profile. It also lists all cut regions by left and right margin (in pixels). The left margins listed here should be entered to paste a cut region back into the display.

Wvparms – This routine is general purpose. It selects data from the array Wvidat and places it into arrays XX and YY.

Vrange – This module is called by option and is used to change the vertical scale of the graphic display. The range of acceptable values is from 1...9 with the value initially set to 2. This scaling parameter can be thought of as using (1/scaling

parameter)th of the vertical display to plot the spectrum. For a value of one, the entire vertical screen is used for display, while for a value of nine, one ninth of the vertical screen is used. The larger the value entered, the more vertically compressed the spectrum looks.

Vshift – This routine is called by option, and is used to enter the amount of the vertical shift for the source spectrum. The shift is in intensity units with a permissible range from 1...5000. The vertical shift is cumulative, adding each new value to the previous. The abs(limit) is 5000 units. This is the module that allows the user to define the magnitude of the vertical shift of the source spectrum relative to the standard spectrum so the continuum can be fit accurately.

Curriculum Vitae

Name:	Kenneth N. Belcourt
Birthplace:	Brunswick, Maine
Birthday:	October 30 1960
Education:	Eastern Connecticut State College, Willimantic Connecticut B.Sc. 1983
	Saint Mary's University, Halifax Nova Scotia M.Sc. 1989 "A High Resolution M Band Study of W3 IRS5"